CHALMERS
UNIVERSITY OF TECHNOLOGY

UNIVERSITY OF GOTHENBURG

An Ultrasonic airspeed sensor prototype for a fixed-wing drone

Master's thesis in Embedded Electronic System Design

Hakim Male

Department of Computer Science and Engineering
CHALMERS UNIVERSITY OF TECHNOLOGY
UNIVERSITY OF GOTHENBURG
Gothenburg, Sweden 2023

MASTER'S THESIS IN EMBEDDED ELECTRONIC SYSTEM DESIGN

An Ultrasonic airspeed sensor prototype for a fixed-wing drone

Hakim Male

Department of Computer Science and Engineering
CHALMERS UNIVERSITY OF TECHNOLOGY
Gothenburg, Sweden 2023

An Ultrasonic airspeed sensor prototype for a fixed-wing drone
Hakim Male

© Hakim Male, 2023.

Supervisor: Arne Linde, Department of Computer Science and Engineering
Company advisor: Richard Kahl, Sigma Embedded Engineering AB
Examiner: Per Larsson-Edefors, Department of Computer Science and Engineering

Master's Thesis in Embedded Electronic System Design
Department of Computer Science and Engineering
Chalmers University of Technology and University of Gothenburg
SE-412 96 Gothenburg
Telephone +46 31 772 1000

Typeset in LaTeX
Printed by Chalmers Reproservice
Gothenburg, Sweden 2023

Abstract

This project explores the development of a low-cost ultrasonic airspeed sensor prototype that can be implemented in fixed-wing drones. The current methods for measuring airspeed, such as the Pitot tubes, have limitations in terms of their usability in low-cost Unmanned Aerial Vehicles (UAV). By exploiting the Doppler shift in ultrasonic sensing, the proposed prototype offers a viable alternative to traditional methods of calculating airspeed.

The prototype comprises an ultrasonic transmitter and two receivers aligned at angles between 30° and 60°, a signal processing circuitry, and a micro-controller. Through systematic experiments, an investigation of the sensor's response to various airspeeds was carried out. The collected data was extensively analysed to evaluate the system's performance, accuracy, and operational range.

The results successfully demonstrate the feasibility of using ultrasonic technology to estimate the airspeed of a fixed-wing drone by operating the transmitter in a pulsed mode setting and the receiver in a scanning mode configuration, applying the Doppler beam swinging method, calculating the resulting frequency shift and thereby deriving the indicated airspeed.

Keywords: Doppler-shift, Doppler beam swinging, Piezoelectric effect, Ultrasonic transducers, Signal filtering

Sammafattning

Detta projekt utforskar utvecklingen av en lågkostnadsprototyp för ultraljudsfartssensorer som kan implementeras i fastvingade drönare. De nuvarande metoderna för att mäta lufthastighet, såsom Pitot-rör, har begränsningar när det gäller deras användbarhet i lågkostnads obemannade flygfordon (UAV). Genom att utnyttja till exempel Doppler-skift i ultraljudsdetektering erbjuder den föreslagna prototypen ett genomförbart alternativ till traditionella metoder för att beräkna lufthastighet.

Prototypen består av en ultraljudssändare och två mottagare riktade i vinklar mellan 30° och 60°, en signalbehandlingskrets och en mikrokontroller. Genom systematiska experiment genomfördes en undersökning av sensorernas respons på olika lufthastigheter. Den insamlade datan analyserades noggrant för att utvärdera systemets prestanda, noggrannhet och operativa räckvidd.

Resultaten visar framgångsrikt genomförbarheten av att använda ultraljudsteknik för att uppskatta flyghastigheten för en fastvingad drönare genom att använda sändaren i ett pulserande inställningsläge och mottagaren i ett skanningsläge.

Nyckelord: Doppler-skiftning, Doppler strålviftning, Piezoelektrisk effekt, Ultraljudssändare, Signalfiltrering

Acknowledgements

I would like to express my gratitude to the following entities for their invaluable support during the development of this thesis.

Firstly, I would like to thank Sigma Embedded Engineering in Lindholmen for having allowed me to do my thesis with them. The support that each and everyone at Sigma contributed and shaped how the prototype eventually developed.

I would also appreciate the support given to me by Fredrik Falkman from the Swedish Sea Rescue Society (SSRS). His guidance helped me tremendously understand the logistics and expected outcome of the project.

Furthermore, I would like to thank Arne Linde, my project supervisor, for his mentorship, guidance, and support throughout the project. His expertise and insights were invaluable in shaping the project's and ensuring its success.

I am deeply grateful to all these individuals and organizations for their support and encouragement. Without their help, this project would not have been possible.

Lastly, i would like to express my utmost gratitude to my examiner, Prof. Per Larsson-Edefors who immensely guided me in putting this thesis report in a better format, so that its message could be easily followed and understood. Thank you very much.

Hakim Male, Gothenburg, October 2023

Abbreviations

I^2C Inter-Integrated Circuit
R_x receiver
T_x transmitter

ADC Analog-to-digital converter

CFD Computational Fluid Dynamics

DAC Digital-to-analog converter
DNL Differential nonlinearity
DSP digital signal processors

EMC Electromagnetic Compatibility
EMI Electromagnetic Interference

FFT Fast Fourier transform
FIR finite impulse response
FPU Floating point unit

GBW Gain bandwidth
GBWP Gain bandwidth product
GPIO general purpose input/output

IC input Capture
IC integrated circuit
IDE Integrated development environment
IIR infinite impulse response
INL Integral nonlinearity

MEMS Micro-electromechanical Systems

PCB Printed Circuit Board
PWM pulse width modulation

SNR signal-to-noise ratio
SPI Serial peripheral interface

ToF Time-of-Flight

UAV Unmanned Aerial Vehicles
USART universal synchronous/asynchronous receiver/transmitter

List of Figures

1.1 Basic forces acting on a flying fixed-wing drone 1
1.2 Different stages of refining the calculated airspeed 2

2.1 Stationary and moving source and observers 8
2.2 Sound-wave propagation from a stationary source (S) 9
2.3 Propagation of sound waves: Source moving from point A to D 10
2.4 Alignment of the T_x and R_x transducers based on motion direction . . 11
2.5 Calculate the hypotenuse to form the basis for the DBS method . . . 12
2.6 Angle of inclination with respect to the direction of motion 12
2.7 Frequency response for an EC4014 transducer at 40 kHz 15

4.1 System Block diagram 22
4.2 The STM32F303K8 micro-controller 23
4.3 Ultrasonic transducer types: transmitter and receiver 24
4.4 Low-pass filter circuitry 25
4.5 Band-pass filter circuitry 28

5.1 Raw unfiltered signal from the receiver 33
5.2 Frequency response bode plot from the low-pass filter 34
5.3 Filtered and unfiltered signal representation 35
5.4 Frequency response curve of the designed bandpass filter 36
5.5 Converting sine wave to square wave 37
5.6 Calculated airspeed vs. anemometer speed reading 38

A.1 Schematic for the sensor prototype I
A.2 Ultrasonic transducers' housing II
A.3 Test platform onto which the housing was mounted III

List of Tables

2.1 Doppler shift calculation synopsis 10
2.2 Calculated $cos(\alpha)$ for every angle of inclination 13

4.1 Cost estimation per item 30

Contents

1 Introduction **1**
- 1.1 Aim and Scope . . . 3
- 1.2 Limitations . . . 3
- 1.3 Related work . . . 4
- 1.4 Thesis outline . . . 5

2 Technical background **7**
- 2.1 Doppler effect . . . 7
  - 2.1.1 Observed frequency due to Doppler shift . . . 8
- 2.2 Doppler beam swinging (DBS) . . . 11
- 2.3 Signal Filtering . . . 13
- 2.4 Ultrasonic transducers . . . 14
- 2.5 Speed of sound in different media . . . 15

3 Methods **16**
- 3.1 Simulation and filter design . . . 16
- 3.2 Physical assembly and adjustments . . . 17
- 3.3 Signal processing . . . 18
- 3.4 Real-time frequency variation analysis . . . 19
- 3.5 Platform design . . . 20
- 3.6 Transmitter design . . . 20
  - 3.6.1 Operational amplifiers . . . 21
- 3.7 Debugging tools . . . 21

4 Design and implementation **22**
- 4.1 Block diagram . . . 22
- 4.2 Hardware components . . . 23
  - 4.2.1 Micro-controller . . . 23
  - 4.2.2 Ultrasonic transducers . . . 24
  - 4.2.3 Passive and active component series . . . 24
- 4.3 Amplification of the transmitter signal . . . 25
- 4.4 Signal reception . . . 25
  - 4.4.1 Low-pass filter . . . 25
  - 4.4.2 Signal buffering . . . 26
  - 4.4.3 Bandpass filter . . . 27
- 4.5 Digital Comparator . . . 29
- 4.6 Calculating the airspeed . . . 29

4.7 Cost estimation 30
4.8 Sensor positioning 31

5 Results **33**
5.1 Micro-controller configuration 33
5.2 Processing the received signal 33
5.2.1 Low-pass design 34
5.2.2 Bandpass filtering and amplification 34
5.2.3 Digitizing the signal 37
5.3 Calculated the airspeed 38

6 Conclusion **39**

7 Future work **40**

Appendix **I**

1

Introduction

The airspeed of a drone is its speed relative to the air in which it is flying [1]. Four forces keep a drone in the sky and are directly affected by the airspeed of the drone while it is airborne. They are weight, lift, thrust, and drag, as shown in Figure 1.1.

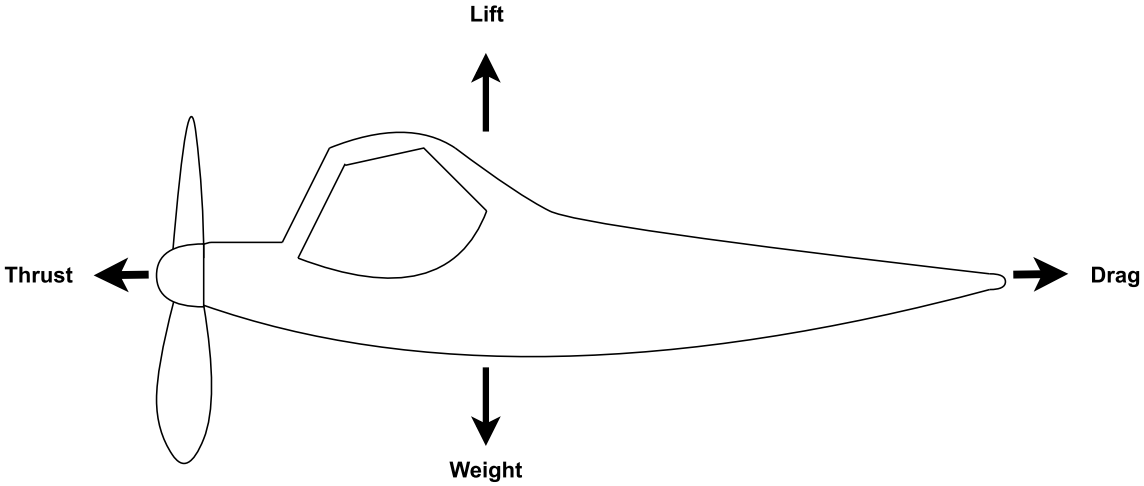

Figure 1.1: *Basic forces acting on a flying fixed-wing drone*

Weight is the force of gravity, acting in the downward direction of motion towards the earth's centre. Lift occurs when the force acts at a right angle to the direction of motion in the air. It is created by differences in air pressure. The force thrust propels a flying drone in the direction of motion and is produced by either an engine or propellers mounted on motors. Drag force acts opposite to the direction of motion and is caused by friction and differences in air pressure [2]. As lift and weight must be equal to maintain a constant altitude, thrust and drag must remain equal to maintain a constant airspeed. This implies that knowing the airspeed at which the drone is flying is always critical to flying and operating it perfectly safely.

The airspeed recorded by the instruments goes through several refining processes before it can be usable by either the pilot or the auto-piloting system that controls the drone.

Figure 1.2 below shows the stages of correcting and refining the airspeed reading to either the true or the ground speed reading. Indicated airspeed (IAS) is the airspeed of the drone measured by other external gadgets like a pitot-static system or any other method and displayed on an airspeed indicator (ASI). The direct instrument

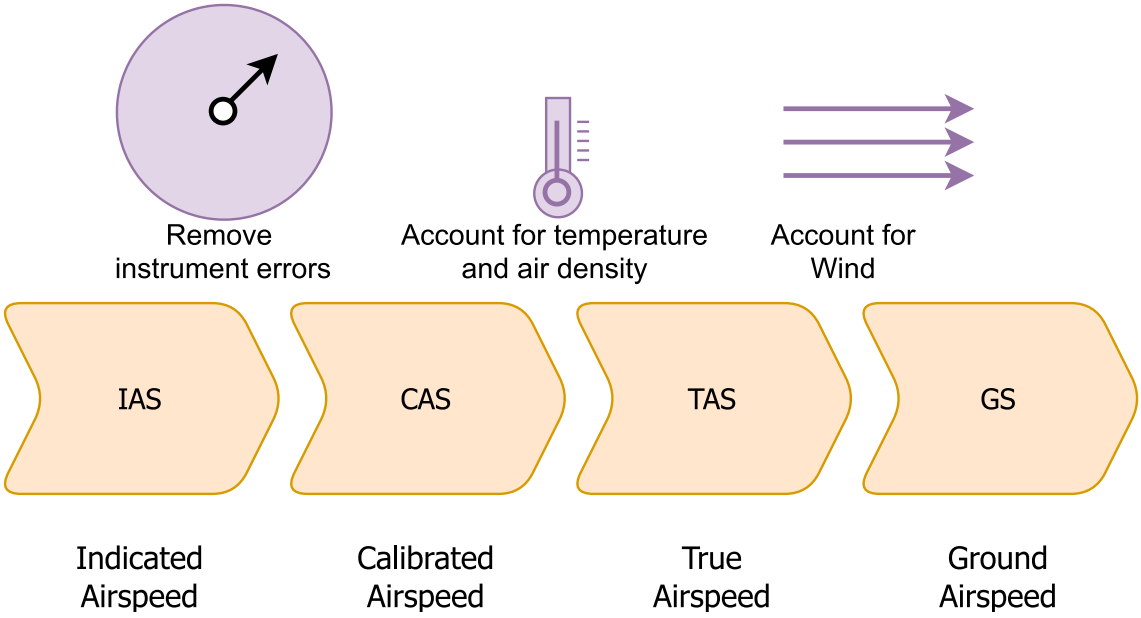

Figure 1.2: *Different stages of refining the calculated airspeed*

reading obtained from the ASI is uncorrected for variations in atmospheric density, installation error, or instrument error [3].

Calibrated airspeed (CAS) is indicated airspeed corrected for instrument and position error. This is because when the drone is flying at sea level under international standard atmosphere conditions of 15^0C, 1013 hPa and 0% humidity, the calibrated airspeed is the same as the equivalent airspeed (EAS) and true airspeed (TAS). So essentially, if there is no wind, it is the same as ground speed (GS) [4]. Furthermore, equivalent airspeed is calibrated airspeed corrected for the possibility of air at a non-trivial Mach number. It is also the airspeed at sea level in the international standard atmosphere at which the dynamic pressure is the same as the dynamic pressure at the true airspeed and altitude at which the drone is flying [4]. It is the speed that is useful in predicting drone handling, aerodynamic loads and stalling, among others.

True airspeed is the speed of a drone relative to the air mass through which it is flying. A drone's true airspeed is crucial for accurate navigation and thus is the speed that truly measures the drone's performance on the cruise and is therefore listed in the drones' specifications and manuals.

In the scope of this thesis, only the indicated airspeed will be dealt with to investigate the feasibility of using ultrasonic sound to measure airspeed.

1.1 Aim and Scope

The main aim of this project is to provide a prototype low-cost sensor solution as an alternative to a pitot-tube system to calculate the airspeed of a fixed-wing drone using ultrasonic sound. The study will address the associated challenges and validate the performance of the prototype with respect to a comprehensive investigation of existing airspeed measurement techniques. Only the indicated airspeed will be calculated at intermittent time intervals in the prototype.

1.2 Limitations

Some various factors and constraints will affect the overall implementation and functioning of the design concept and are, therefore, listed below.

- Computational Fluid Dynamics (CFD): CFD have not been performed on the prototype as it requires significant computational resources, time, and specific expertise that may not be feasible to include in developing a basic prototype. Therefore, the initial focus is on validating the concept of ultrasonic airspeed detection, with the potential for CFD analysis in subsequent iterations or optimisation stages of the prototype.
- Although Electromagnetic Compatibility (EMC) & Electromagnetic Interference (EMI) are crucial for reliable and accurate electronic performance, they have been considered beyond the scope of this prototype mainly due to the complexity and resources required for their thorough analysis on the final Printed Circuit Board (PCB). The emphasis is, therefore, put on the functionality, proof-of-concept, and performance of the ultrasonic airspeed sensor. Follow-up studies could be conducted to address these concerns.
- Temperature Constraints: All simulations and implementations will be carried out at room temperature 21–25 °C. This constraint will ensure that component temperature tolerances, such as those of resistors and op-amps, remain within acceptable limits, providing consistent and accurate results during simulations and prototyping. Although this may limit the prototype's performance in real-world applications with varying temperatures, validation of the core concept is deemed more important in this stage of development.
- Environmental Factors such as humidity, dust, and precipitation are not considered in the prototype. Such factors may limit the prototype's effectiveness in real-world scenarios.
- Acoustic Properties: The material through which the ultrasonic waves propagate can influence the sensor's accuracy. For example, the speed of sound varies in different gases or mixtures and at given temperatures. This project assumes a relatively constant air composition and will not address these variances' impact on the sensor's accuracy.
- Noise Immunity and Filtering: The prototype's capability to handle and filter different types of noise, intrinsic and extrinsic, will not be explored. This lim-

itation may affect the sensor's performance in real-world applications where variable noise sources are expected.

- Integration with a Fixed-wing Drone: The project's current scope is focused on developing and validating the airspeed sensor prototype, and it does not necessarily address integration with existing fixed-wing drone systems. This limitation may require further study to ensure seamless integration, coordination, and data sharing with the drone's flight controller and other onboard sensors.
- Power Consumption and Battery Life: An analysis of power consumption and battery life implications for varying drone configurations has not been considered within this project. However, an initial limit of 400 mW was established to provide a reference for further improvements.

1.3 Related work

In a novel design for UAV, microphones were placed on the vehicle's nose cone to capture pseudo-sound produced by the flow structures [5]. The researchers hoped to subtract acoustic sounds from the microphone recordings but found the pseudo-sound overpowered the recordings, rendering the subtraction method ineffective, although, in another study, neural networks were trained to relate the microphones' signal power spectral density (PSD) to the airspeed measured by a pitot tube in a wind tunnel. Interestingly, using only the left-mounted microphone's signal achieved the lowest approximation error compared to subtracted signals, indicating that signal subtraction was unnecessary. The best model had a root mean square error of $1.037\,\mathrm{m\,s^{-1}}$.

In another study, a means was developed to determine the actual speed of a vehicle using the Doppler effect of an ultrasonic wave [6]. They showed that ultrasonic waves with a frequency of 200 kHz applied to determine the actual speed of a vehicle within a practical precision of 5% in the range of 0–50 $\mathrm{km\,h^{-1}}$.

The market has several airspeed sensors with unique features, advantages, and limitations. These include pitot tubes, which are the oldest and most widely used airspeed sensing technologies, and the laser Doppler anemometer, which measures airspeed by emitting a laser beam and analyzing scattered light from airborne particles (e.g., dust and water droplets) moving with the air. The hot-wire anemometer, another airspeed sensor, is based on convective cooling of a heated wire and then measures airspeed by detecting heat loss due to airflow. The acoustic Doppler velocimetry [7] that is utilized in ultrasonic techniques measures airspeed by emitting acoustic waves and detecting the Doppler shift in frequency as they are reflected off moving air particles within the airflow.

Each of the above airspeed sensing technologies has specific trade-offs, making them more or less suitable for specific fixed-wing drone applications. Common lim-

itations that may impact the performance and reliability of a given method include accuracy, sensitivity to environmental factors, including dust, ice, humidity, or even insects, and maintenance to ensure consistent performance.

In the case of fixed-wing drones, effective airspeed detection is paramount to maintain stability, trajectory control, and energy optimization [8]. Conventional airspeed measurement techniques, such as pitot-static systems, have been widely used in the aviation industry. Although these systems have served the industry well, they face several limitations and inaccuracies caused by environmental factors, such as ice accumulation and pressure variations [8]. This has spurred the need for alternative airspeed sensing technologies.

The interest in ultrasonic airspeed sensing is rooted in several advantages that ultrasonic sensors offer over traditional methods. Their non-contact nature, high accuracy, lightweight, and reduced sensitivity to environmental factors make them an advantageous choice for UAV applications [8]. Ultrasonic anemometers, mainly used for meteorological and industrial applications [9], have been gaining attention for their potential use in fixed-wing drones. However, they measure wind speed and not speed, where both the source of the sound waves and the observer are mounted on the same platform and moving at the same rate.

The principles of ultrasonic detection consist of measuring the difference Time-of-Flight (ToF) in ultrasonic waves between two or more transducers [10, 11]. In the context of distance, this ToF difference is influenced by airflow, allowing the determination of airspeed based on the time difference between forward and backward propagation of ultrasonic signals [12]. Ultrasonic anemometers have demonstrated their ability to measure airflow under various conditions accurately [13], indicating their potential to revolutionize airspeed detection for fixed-wing drones.

However, sensors specifically for UAV where Micro-electromechanical Systems (MEMS) based ultrasonic airspeed sensor for micro UAV applications was designed [14], showed that integrating and optimizing an ultrasonic airspeed sensor for fixed-wing drones involved addressing various challenges, tests, and comparisons, presenting fertile ground for further research and advancement.

1.4 Thesis outline

This report provides comprehensive information on designing and developing an ultrasonic airspeed sensor prototype for a fixed-wing drone. Chapter 1 sets the foundation for the project by outlining the objectives, motivation, and significance of the prototype developed, as well as presenting the scope and relevance of the project to the drone industry. Chapter 2 delves into the fundamental concepts that underpin the operation of the ultrasonic airspeed sensor. Chapter 3 outlines the comprehensive process of designing and testing the airspeed sensor prototype, focusing

on simulating and creating filters, assembling physical components, processing signals, conducting real-time frequency difference calculations, developing a specifically designed 3D printed platform, scrutinizing filter performance, and eventually, constructing an effective transmitter. Chapter 4 provides a detailed account of the design process by describing critical components, design considerations, and the rationale behind each decision. In Chapter 5, the results of the design and verification phases are presented. Here, experimental verification and system analysis assess the ultrasonic airspeed sensor prototype's performance, accuracy, and reliability. In Chapter 6, a summary of the achievements, key findings, and contributions of the project is provided. It also offers insights into future directions and potential improvements to enhance the prototype's performance and applicability.

2

Technical background

A thorough understanding of the underlying technical principles is the key to a successful and reliable ultrasonic airspeed sensor prototype. This section provides an in-depth exploration of fundamental concepts that play a critical role in the design and operation of the airspeed sensor.

2.1 Doppler effect

The Doppler effect, or Doppler shift, is the apparent change in frequency of a wave with respect to an observer moving relative to the wave source. [15]. It was named after the Austrian physicist Christian Doppler, who described the phenomenon in 1842. A typical example of a Doppler shift is the change of pitch heard when a vehicle sounding a horn approaches and recedes from an observer. Compared to the emitted frequency, the received frequency is higher during the approach, identical at the instant passing by, and lower during recession [16].

The cause of the Doppler effect is that when the source of the waves is moving towards the observer, each successive wave crest is emitted from a position closer to the observer than the crest of the previous wave. As the source of the waves moves towards the observer, the range of each successive wave is emitted from a position closer to the observer than the crest of the previous wave. Thus, each wave takes slightly less time to reach the observer than the last one [16, 17].

Sounds waves emitted by a source spread out in spherical waves Figure 2.1a. When the source, observers, and air are stationary, the wavelength and frequency are the same in all directions and to all observers. Sounds emitted by a source moving to the right spread out from the points at which they were emitted. The wavelength is reduced, and consequently, the frequency is increased in the direction of motion so that the observer on the right hears a higher-pitched sound. The opposite is true for the observer on the left, where the wavelength is increased and the frequency is reduced. The same effect is produced when the observers move relative to the source. Motion toward the source increases frequency as the observer on the right passes through more wave crests than she would if stationary. Movement away from the source decreases frequency as the observer on the left passes through fewer wave crests than if fixed.

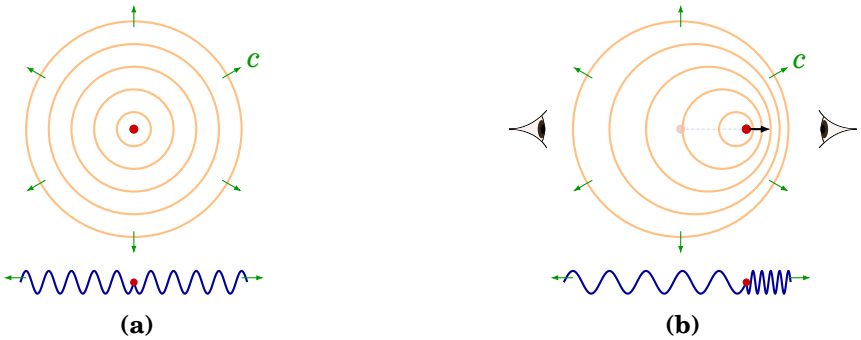

Figure 2.1: *Stationary and moving source and observers*

The speed of sound in a given media C, the frequency of the wave f, and its wavelength λ are related in the formula below [18],

$$C = f \cdot \lambda \tag{2.1.1}$$

where:

The sound moves in a medium with the same speed v in that medium, whether or not the source is moving. Thus, f multiplied by λ is a constant. Because the observer in Figure 2.1b receives a shorter wavelength, the frequency she receives must be higher. The relative motion of the source and observer toward one another generally increases the received frequency. Relative motion apart decreases frequency. The higher the relative speed, the greater the effect. The Doppler effect occurs for sound and any wave when relative motion between the observer and the source occurs. Doppler shift occurs in the frequency of sound, light, and water waves, and it can be used to determine velocity, such as when ultrasound is reflected from blood in a medical diagnostic [19]. The relative velocities of stars and galaxies are determined by the shift in the frequencies of light received from them and have revealed much about the universe's origins.
So therefore, the general formula for the Doppler shift is

$$\text{Doppler Shift}_{(Hz)} = \text{Frequency}_{(Rx)} - \text{Frequency}_{(Tx)} \tag{2.1.2}$$

2.1.1 Observed frequency due to Doppler shift

Consider two stationary observers, X and Y, in Figure 2.2, located on either side of a stationary source. Each observer hears the same frequency, and that frequency is the frequency produced by the stationary source. A stationary source sends out sound waves at a constant frequency f_s with a continuous wavelength λ_s, at the speed of sound V. On either side of the source, two stationary observers X and Y observe a frequency $f_o = f_s$, with a $\lambda_o = \lambda_s$ wavelength. Using the fact that the wavelength is equal to the speed times the period and the period is the inverse of the frequency, we can derive the observed frequency.

A sound emitting source moving at a constant speed v_s away from an observer X sends out sound waves at a continuous frequency f_s with a continual wavelength λ_s at a rate of sound v. Snapshots of the source in motion at an interval of T_s are taken

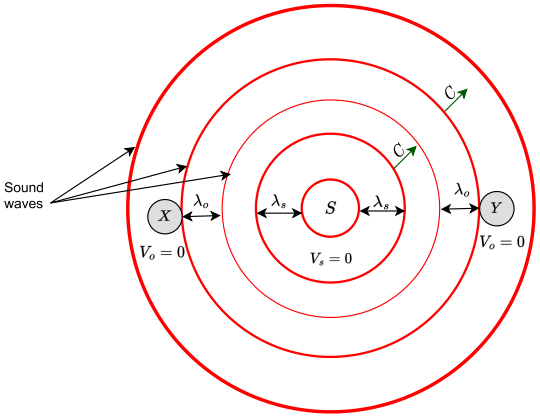

Figure 2.2: *Sound-wave propagation from a stationary source (S)*

as in Figure 2.3. The solid lines represent the position of the sound waves after four periods from the initial time. The dotted lines show the parts of the waves at each period. The observer hears a wavelength of

$$\lambda_o = \lambda s + \Delta x = \lambda_s + v_s \cdot T_s \tag{2.1.1.3}$$

Using the fact that the wavelength is equal to the speed times the period, and the period is the inverse of the frequency, we can derive the observed frequency:

$$\begin{aligned} \lambda_o &= \lambda_s + \Delta X \\ v \cdot T_o &= v \cdot T_s + v_s \cdot T_s \\ \frac{v}{f_o} &= \frac{v}{f_s} = \frac{v_s}{f_s} = \frac{v + v_s}{f_s} \\ f_o &= f_s \cdot \left(\frac{v}{v + v_s} \right) \end{aligned} \tag{2.1.1.4}$$

Solving for $f_{observer}$

We can see from Equation 2.1.1.4 that mathematically, as the source moves away from the observer, the observed frequency is lower than the source frequency.

Consider a stationary observer X with a source moving away from the observer with constant speed V_s in Figure 2.2. At time $t = 0$, the source sends a sound wave. This wave spreads out at the speed of sound $V$the position of the sound wave at each time interval of the period T_s. After a period, the source has moved $\Delta x = v_s \dot{T}_s$ and emits a second sound wave that moves at the speed of sound. The source continues to move and produces sound waves, as indicated by the circles in the figure. Notice that as the waves move out, they remain centred at their respective point of origin.

When we consider a source moving at a constant velocity v_s, moving towards a stationary observer X shown in Figure 2.3, the wavelength is observed by Y as

$$\lambda_o = \lambda_s - \Delta x = \lambda_s - v_s \cdot T_s \tag{2.1.1.5}$$

So when the source is moving, and the observer is stationary, the observed frequency is the same as in Equation 2.1.1.4 but changes to count for the possibility

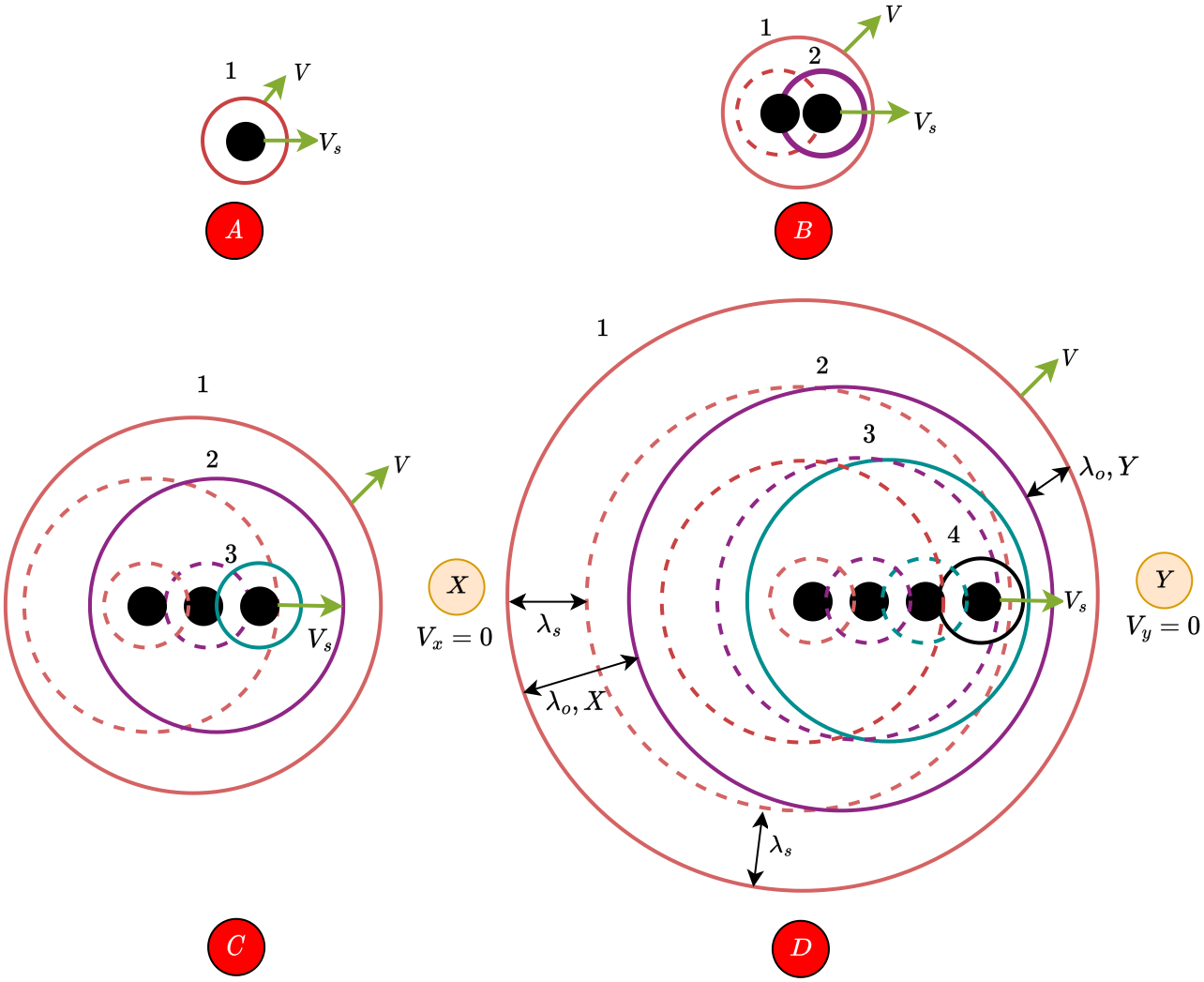

Figure 2.3: *Propagation of sound waves: Source moving from point A to D*

of lower or higher frequencies than those perceived from the source. Thus, we can deduce that;

$$f_o = f_s \cdot \left(\frac{v}{v \pm v_s}\right) \tag{2.1.1.6}$$

The Doppler shift can therefore be summarized as follows;

	Stationary observer	**Observer moving towards source**	**Observer moving away from source**
Stationary source	$f_o = f_s$	$f_o = f_s\left(\frac{v + v_o}{v}\right)$	$f_o = f_s\left(\frac{v - v_o}{v}\right)$
Source moving towards observer	$f_o = f_s\left(\frac{v}{v - v_s}\right)$	$f_o = f_s\left(\frac{v + v_o}{v - v_s}\right)$	$f_o = f_s\left(\frac{v - v_o}{v - v_s}\right)$
Source moving away from observer	$f_o = f_s\left(\frac{v}{v + v_s}\right)$	$f_o = f_s\left(\frac{v + v_o}{v + v_s}\right)$	$f_o = f_s\left(\frac{v - v_o}{v + v_s}\right)$

Table 2.1: *Doppler shift calculation synopsis*

2.2 Doppler beam swinging (DBS)

The Doppler shift introduced in section 2.1 works under the circumstance that either the transmitter (T_x) or the receiver (R_x) are stationary relative to each other or that both elements are moving at different speeds. But since the prototype is to be mounted on a moving platform, a fixed-wing drone in this case, both the T_x and R_x will be mounted on the same platform, which indicates that they will be moving at the same speed, and in the same direction. This renders the Doppler shift technique ineffective, and hence, a more robust method, Doppler beam swinging, is employed to calculate the airspeed.

This technique is often considered advantageous over the primary Doppler effect when both the source (T_x) and observer (R_x) are in motion. This allows for more accurate measurements and improved direction estimation. It involves sweeping or swinging the direction of the transmitted beam across the target area. By analyzing the Doppler shift in the received signal at different beam angles, one can estimate the velocity and direction of the moving object.

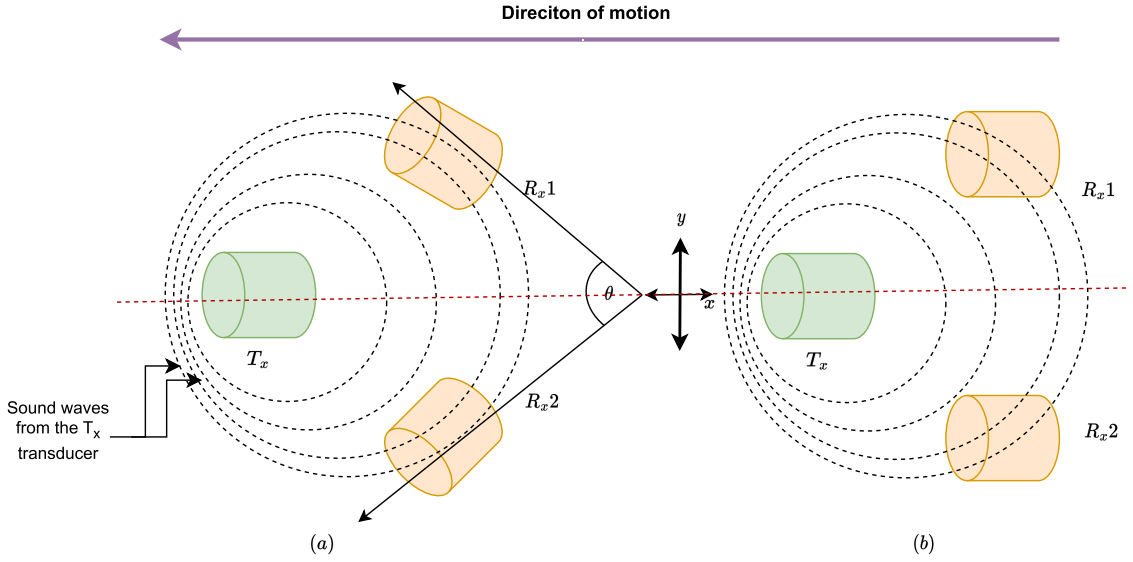

Figure 2.4: *Alignment of the T_x and R_x transducers based on motion direction*

By using multiple receivers set at different angles, more data points are available in the space plane for analysis (Figure 2.4 (a)). This allows for better accuracy in estimating the Doppler shift and, consequently, the speed or velocity of the moving object. It is challenging to accurately estimate the Doppler shift with a single receiver when both the source and the observer are in motion.

Each receiver is to be put at an angle of inclination $\theta/2$ to the direction of the beam source. If we were to get rid of that angle so that the receiver transducers face directly in the same direction as the transmitter transducer (Figure 2.4 (b)), then the Doppler shift equation would be

$$\text{Doppler shift}_{(Hz)} = 2 * F_{Tx} * \frac{\text{Speed}_{Rx}}{\text{Speed}_{Sound}} \tag{2.2.7}$$

By using trigonometry, we can calculate the platform's velocity if we know the angle of inclination $\theta/2$, which, in our case, is known from the platform's architecture. Taking the adjacent side of the right-angled triangle ABC in Figure 2.5, we can

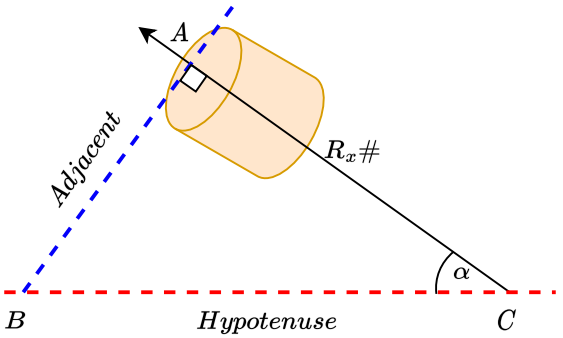

Figure 2.5: *Calculate the hypotenuse to form the basis for the DBS method*

calculate the the hypotenuse as

$$\cos(\alpha) = \frac{A}{H} \qquad \text{Solving for } A \qquad A = H * \cos(\alpha) \tag{2.2.8}$$

To compensate for the angle of inclination, we substitute Equation 2.2.8 into Equation 2.2.9 and therefore the Doppler shift

$$\text{Doppler shift}_{(kHz)} = \frac{2 * F_{Transmitter} * H * \cos(\alpha)}{\text{Speed of sound (C)}} \qquad \text{Solving for } H \qquad H = \frac{\text{Frequency}_{Doppler} * C}{2 * \text{Frequency}_{Transmitter} * \cos(\alpha)} \tag{2.2.9}$$

Hypotenuse, or velocity in this case, is no longer a scalar. It has magnitude and direction, and therefore it is a vector. The $\cos(\alpha)$ allows us to add the directional component. We can also see from Equation 2.2.9 that as the velocity of the fixed-wing drone increases, the Doppler shift increases, too. As the angle of inclination α increases, the $\cos(\alpha)$ value will also decrease. As the angle of inclination increases, the Doppler shift will decrease, and therefore, the magnitude of the scalar value (Adjacent) will decrease.

The angle of inclination α will also determine how much of a Doppler shift the receivers capture, as it must lie within a suitable range.

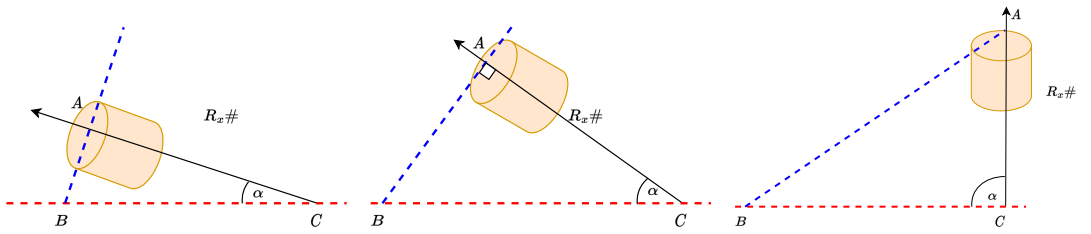

(a) 30^0 **(b)** 60^0 **(c)** 90^0

Figure 2.6: *Angle of inclination with respect to the direction of motion*

Angle	α
0	1
30	0.87
45	0.7
60	0.5
80	0.17
90	0

Table 2.2: *Calculated $cos(\alpha)$ for every angle of inclination*

We can see from Table 2.2 that when the ultrasound transducer probes' angle of inclination is close to zero degrees, as in less than in Figure 2.6a, then the $\cos(\alpha)$ tends towards 1. This means that the observed Doppler shift is directly proportional to the drone's velocity, according to Equation 2.2.9. The $\cos(\alpha)$ decreases as the inclination angle increases. Therefore, an increase in the Doppler angle will decrease the Doppler shift.

When the transducer is at a 30^0 angle to the direction of motion, the calculated Doppler shift will be 0.87 of the actual value of the drone's velocity. When that value reaches 60^0, the Doppler shift will be 0.5, or half the actual velocity value we seek.

Because we are dealing with adjacent and hypotenuse in the cosine calculation, we cannot have the ultrasonic transducers aligned perpendicular to the flow of movement (Figure 2.6c). We will not be able to measure any Doppler shift at this 90^0 angle at all because $\cos(90) = 0$.

At very steep angles, we run into refraction problems, so generally, an angle between 30–60° is preferable to get an accurate calculation that doesn't have the problem of refraction (below 30^0), as well as having the issue of **angle correction** that occurs at close to 90^0.

2.3 Signal Filtering

Filtering of signals is a fundamental signal processing technique used to modify or extract specific information from a signal. It involves the application of mathematical operations or algorithms to selectively attenuate or emphasize specific frequency components or characteristics within the signal [20].

Filters are commonly used to remove unwanted noise, extract relevant information, reduce interference, or shape the frequency response of a signal. They can be divided into two main types: analog filters and digital filters.

Analog filters operate on continuous-time signals and employ passive components (resistors, capacitors, and inductors) or active components (operational amplifiers) to manipulate signal characteristics. Common types of analog filters include low-pass filters, high-pass filters, band-pass filters, and band-reject filters. They are widely used in various applications, including audio processing, communication systems, and instrumentation.

Digital filters, on the other hand, process discrete-time signals obtained by sampling continuous-time signals. They are implemented using digital signal processing algorithms executed on computing platforms, such as micro-controllers or digital signal processors (DSPs) [21]. Digital filters offer advantages such as precise control, flexibility, programmability, and the ability to handle complex signal-processing tasks efficiently.

Digital filters can be further classified into finite impulse response (FIR) and infinite impulse response (IIR) filters. FIR filters have a finite-duration impulse response, meaning their output depends only on a finite number of previous input samples. They provide linear phase characteristics, good stability, and simple implementation. IIR filters have an infinite-duration impulse response and exhibit feedback in their structure. They offer efficient implementation but may introduce non-linear phase distortions.

The design and implementation of filters involve considerations such as the desired frequency response, filter order, filter type, cutoff frequencies, stop-band attenuation, and transition bandwidth. Different filter design techniques, such as windowing, Fourier analysis, or optimization algorithms, can be utilized to achieve specific filtering objectives. The appropriate choice and design of a filter depend on the characteristics of the input signal, the desired output, and the particular requirements of the application at hand.

2.4 Ultrasonic transducers

Ultrasonic transducers typically use piezoelectric materials to convert electrical energy into mechanical vibrations and vice versa. Piezoelectric materials exhibit the property of generating an electric charge when mechanically stressed and deforming when an electric field is applied. The piezoelectric material sits at the front of the transducer, and it is the one that creates the ultrasound waves as well as receives them, depending on the configuration of the transducer. The piezo crystal ($Pb(ZrTi)O_3$) is made up of unique properties [22] that will induce movement as soon as a mechanical vibration is sensed or induced in someway.

The piezo material is fabricated and always has a diameter or length that will not change under its lifetime operation [23]. The material has a resonance at a set frequency, and the broader or bigger the material's radius, the smaller the frequency it generates, and vice versa. This means that the ultrasonic transducer controls

the frequency and can be changed by altering the wavelength of the generated frequency. This, however, is not possible with all transducers. Figure 2.7 shows the resonance frequency of the ultrasonic transducer type used in the prototype design. We can see that at around 40 kHz, the transducer is most sensitive to sound waves or an electric signal within that same frequency and will resonate.

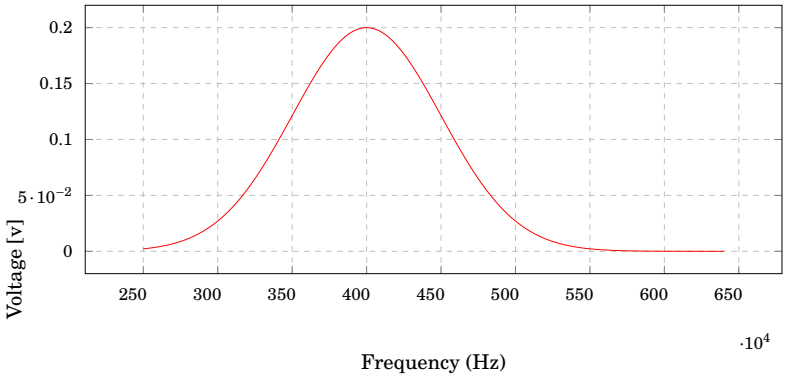

Figure 2.7: *Frequency response for an EC4014 transducer at* 40 kHz

2.5 Speed of sound in different media

In exploring sound's properties, we delve into aspects such as speed, frequency, wavelength, and how they fluctuate across different media and with changing temperatures. Sound, a type of wave, travels at a finite speed which is substantially slower compared to light. Importantly, this speed isn't constant, rather, it relies on aspects of the medium it's traversing primarily the density and compressibility. The relationship between wave speed (V), frequency (f), and wavelength (λ) is expressed as

$$V = f * \lambda \tag{2.5.10}$$

The speed of sound differs among various media such as gases, liquids, and solids. In the air, for example, the speed of sound is sensitive to temperature changes. At 0 °C (273 K), it clocks at approximately $331\,\mathrm{m\,s^{-1}}$ [24]. A useful formula for estimating the speed of sound in air, depending on temperature, is

$$V = 331\,\mathrm{m\,s^{-1}} * \sqrt{\frac{T}{273\,\mathrm{K}}} \tag{2.5.11}$$

where, T is the temperature in Celsius. A unique attribute of sound in the open air is that its speed is almost irrespective of its frequency.

The properties of sound waves undergo alterations when they pass from one medium to another: While frequency stays consistent, the speed and thus, the wavelength of the wave change according to the new medium [24].

3

Methods

The approach to designing an ultrasonic airspeed sensor prototype for a fixed-wing drone involves several key steps. First, a thorough literature review is conducted to fully grasp the current state of the art in ultrasonic airspeed sensor technology, including prior studies and existing commercial sensors. This provides valuable information on the challenges and limitations associated with ultrasonic airspeed sensors and the best practices for designing and testing such sensors.

Next, a conceptual design of the ultrasonic airspeed sensor is developed, keeping in mind the specific requirements for a fixed-wing drone, such as accuracy, power consumption, size, and weight. This includes selecting appropriate components, such as the types of ultrasonic transducers, the signal processing module, and the data acquisition system.

After the conceptual design is complete, the ultrasonic airspeed sensor prototype is constructed and tested. This involves assembling the sensor components and calibrating the sensor to ensure accurate estimations of the airspeed measurement.

Lastly, the test results are analysed to refine the design for better calibration and approximation of the airspeed calculation. Based on these results, sensor components, signal processing algorithms, or data acquisition systems are modified to enhance the prototype's performance gradually.

The development process adhered to an iterative model, a systemic and cyclical method by which different phases of the project development gradually build upon each other. This approach enabled the careful execution of each step, from signal generation to micro-controller integration. It was particularly beneficial in implementing adjustments and refining the design based on inherent challenges observed in each phase.

3.1 Simulation and filter design

This phase made use of LTSpice [25], a popular software tool in electronic engineering for its efficiency and precision. A digital lowpass and bandpass filter were

designed using this software, incorporating all related components required for its functioning.

The filter was put through a simulation process inside this software environment, where the different values of its components, such as resistors and capacitors, were identified and specified on the software interface. One primary focus in this stage was the adjustment of the theoretical values of these components.

Simulating the filter behaviour made it possible to analyze their performance under different conditions, mainly the cut-off frequencies and bandwidth. These parameters are pivotal for the practical functionality of the system. Adjustments were made by modifying the components' values to ensure the filter worked within these specific parameters.

At the end of this section, the cut-off frequencies and bandwidth were noted down from the simulation results, which set the stage for the physical assembly and necessary adjustments that would follow in the later sections. This simulation process enabled the digital validation of the filter design before proceeding to its real-world implementation.

3.2 Physical assembly and adjustments

Upon concluding the digital simulations and achieving the desired results, the study moved toward the practical phase, involving the physical assembly of the bandpass filter along with other components of the prototype.

A fundamental task in this phase was the generation of a pulse width modulation (PWM) signal with a frequency of 40KHz. To confirm the precision of this signal, an oscilloscope was used. This instrument, which visually displays varying signal voltages, verified the integrity of the generated signal. Furthermore, an Analog Discovery was utilized to validate the quantitative aspects of the signal. This multifunction instrument, which integrates the functionalities of multiple devices such as an oscilloscope and waveform generator, helped confirm whether the signal frequency deviated within acceptable limits.

After the successful generation and verification of the signal, the next focus was on the receiver aspect of the prototype. An innovative approach was undertaken for this by making use of an HC-SR04 [26] distance sensor, mounted on a separate micro-controller. The sensor, known primarily for its distance-sensing capabilities in robotics, operates on a similar principle as required for this study. Even though it was not used in its typical capacity for providing distance measurements, it was configured to run continuously, simulating the ultrasonic acoustic sound wave that the final prototype was expected to receive.

This arrangement with the HC-SR04 distance sensor was coupled with stand-alone EC4014 sensors. These sensors, which resonate at the same frequency as those on the HC-SR04, were imperative to study the response of the receiving system to

the incoming acoustic signals. The signals captured from the EC4014 sensors were probed and then amplified for a more detailed analysis.

An important aspect that was looked into was the fine-tuning of the incoming signal. A low-pass filter was applied to the incoming signals in two stages. Firstly, the Analog Discovery was employed to apply the filter digitally, which enhanced the details of the signal. Following this, a physical LP filter was built and integrated into the system, enhancing the signal processing capabilities.

Throughout the assembly process, potential variabilities between the components were observed. Necessary adjustments were carried out to align the component values with those concluded from the simulation phase, as per Section 1. By the end of this phase, the system was ready, with both the practical assembly of the filter and the initial system setup prepared for the next stages of signal processing and experimentation on the fixed-wing drone.

3.3 Signal processing

Having completed the physical assembly, the project moved onto the phase of signal processing, playing a crucial role in shaping the accuracy and efficiency of the ultrasonic airspeed sensor.

The first important step in this stage was implementing the previously designed bandpass filter. This served to minimize any frequencies outside the desired range, thereby limiting signal processing to the most relevant data and contributing to the overall precision of the system. The signal that passed through the filter was then sent to an amplifier, exponentially increasing the amplitude of the filtered signal, and making it easier to work with in the subsequent steps.

In a bid to raise the usability of the signal and extract the maximum possible information from it, a comparator was incorporated. The comparator digitized the signal by converting the incoming analog signal into a binary format, easing the management and interpretation of the data. This digitization was a critical step, as it facilitated the interfacing of the amplified and filtered analog signal with digital components further in the process, particularly the micro-controller.

This stage was also crucial for filter testing, where both lowpass and bandpass filters were put into focus. These filters form the backbone of the functioning of the system, and hence, their comprehensive testing was crucial for understanding their effectiveness and operational efficiency within the prototype system.

The Analog Discovery's network analyzer module, known for its capability to conduct advanced routine network tests, was extensively employed for this operation. The module allowed for an in-depth analysis of the filter's performance in real-world

conditions, bridging the gap between the theoretical and the practical aspects of the system. This testing approach offered invaluable insights into the filters efficiency beyond the confines of controlled simulations and laid out its performance in realistic operational scenarios.

To achieve a higher degree of control in this filter testing process, potentiometers were incorporated into the setup. These devices allowed for the precise tuning of the cutoff frequencies of both the lowpass and bandpass filters. This meant the cutoff frequencies could be manually manipulated to comply with the specific desired frequency range of the system. Taking this approach provided flexibility to adjust filter characteristics in real-time, bringing further depth and accuracy to the testing process.

The goal of this intensive testing process was to validate the performance of these filters and to ensure the cutoff frequencies adhered to the set requirements of the prototype. These tests enabled the observation and fine-tuning of the filters' operation, leading to higher system efficacy and robustness.

Concluding this phase, a comprehensive examination of the lowpass and bandpass filters was achieved, validating their performance and effectiveness.

3.4 Real-time frequency variation analysis

With the successful completion of the signal processing stage, the design delved into a rigorous experimentation phase where two squares were generated using the Analog Discovery tool, both set at 40 kHz. The analog discovery, with its multifunctional instruments, provided an effective way to create, control, and analyze these waveforms.

This phase aimed to evaluate how the input-capture mode of the timer periphery of the micro-controller reacted to varying input frequencies. To achieve this, one of the 40 kHz square waves was flexibly manipulated, changing its frequency between a range 30–40 kHz. This shift in frequency was planned and executed in a systematic manner, maintaining precise control over the pace and range of frequency variation. The endeavour was to discern differences in frequency between the input signals and understand how well and accurately those differences could be calculated in real-time.

The microcontroller's ability to calculate the frequency difference between the incoming signals in real-time constituted one of the main benchmarks of this stage. The findings from this testing would ultimately determine the sensor system's capability of promptly and accurately determining airspeed variation in real applications.

Furthermore, this phase utilized multiple tools and equipped the study with important findings on the performance of the prototype in different potential scenarios. These tests also provided crucial insights into the possibilities and limitations of the implemented system design.

Conclusively, extensive experimentation during this phase played a pivotal role in determining the efficacy of the functional design and understanding the fine-tuning adjustments required to improve its overall performance. Based on these results, final modifications were made to the prototype design, contributing to its readiness for subsequent sections.

3.5 Platform design

The tangible component of the ultrasonic airspeed sensor prototype necessitated the creation of a suitable platform. This platform was tasked with housing the transducers, forming an integral part of the system's physical layout. Given the criticality of correct physical assembly to the overall operation and results of the system, attention to detail in platform design was of utmost importance.

To fashion the platform, cutting-edge 3D printing technology was utilized. The use of 3D printing enabled precise control over the design parameters and provided a seamless, efficient pathway to materialize the envisioned model. Basing the design on the specific requirements of the prototype, the platform was meticulously created to ensure a perfect fit for the transducers.

Careful consideration was given to positioning the transducers, aiming for optimal signal transmission and reception. To this end, various models were tried and tested, and modifications were made as necessary, taking into account factors such as space, angle, and secure mounting.

3.6 Transmitter design

Building upon the previous sections, the process culminated in the design and construction of the transmitter which marked a significant step towards completing the prototype.

The design process started with creating a 40KHz sinusoidal wave using Analog Discovery. However, the Analog Discovery can only produce a sinusoidal wave with a maximum peak-to-peak voltage of 5V, which appeared to be insufficient for the requirements of this sensor system. To overcome this limitation, the signal was relayed to an amplifier, consequently raising the peak-to-peak voltage to 15V, thereby substantially boosting the signal's strength to meet the demands of the system.

Mindful of the specifications of the transducer, such as its maximum voltage rating of 20Vrms and capacitance of 2 nF, attempts were made to increase its Vrms by adjusting the peak-to-peak voltage. These adjustments aimed to raise the sound pressure to upgrade signal reception. Performing a detailed analysis involving calculating the impedance and the current, however, unveiled limitations around power supply capacity. Consequently, the peak-to-peak voltage was maintained at 15V.

3.6.1 Operational amplifiers

The key determining factors that were followed when it came to the choice of operational amplifiers were availability, power consumption, and overall, the Gain bandwidth product (GBWP), which is the ability of an Op-amp to amplify signals at high frequencies. The GBWP determines the frequency range over which the Op-amp can be used. For example, if an Op-amp has a GBWP of 1 MHz, it can amplify signals up to the 1 MHz without significant attenuation. However, the Op-amp gain will roll off if a signal is above 1 MHz.

3.7 Debugging tools

A non-intrusive tool that preserved the real-time behaviour and advanced debugging called STMStudio [27] was used for data visualisation inside the micro-controller. As for the testing and debugging of the physical filters, a multi-function instrument from Digilent called the Analog Discovery [28] was used to measure, record and generate analog and digital signals was used.

4

Design and implementation

This chapter outlines the construction and realization of an ultrasonic sound prototype for calculating the airspeed of a fixed-wing drone. Accurately measuring airspeed is crucial for flight control and navigation systems in UAV. Traditional airspeed measurement methods, such as pitot tubes, may not be suitable for small, lightweight drones due to their added weight and vulnerability to damage.

By employing ultrasonic sound waves, the prototype aims to determine the relative airspeed of the fixed-wing drone by measuring the Doppler effect of sound pulses. This approach offers advantages such as reduced weight, improved durability, and lower complexity than traditional methods.

4.1 Block diagram

The block diagram presented in Figure 4.1 illustrates the overall architecture and flow of the ultrasonic sound prototype for airspeed calculation of the drone. The diagram showcases the two main subsystems: signal generation and signal reception.

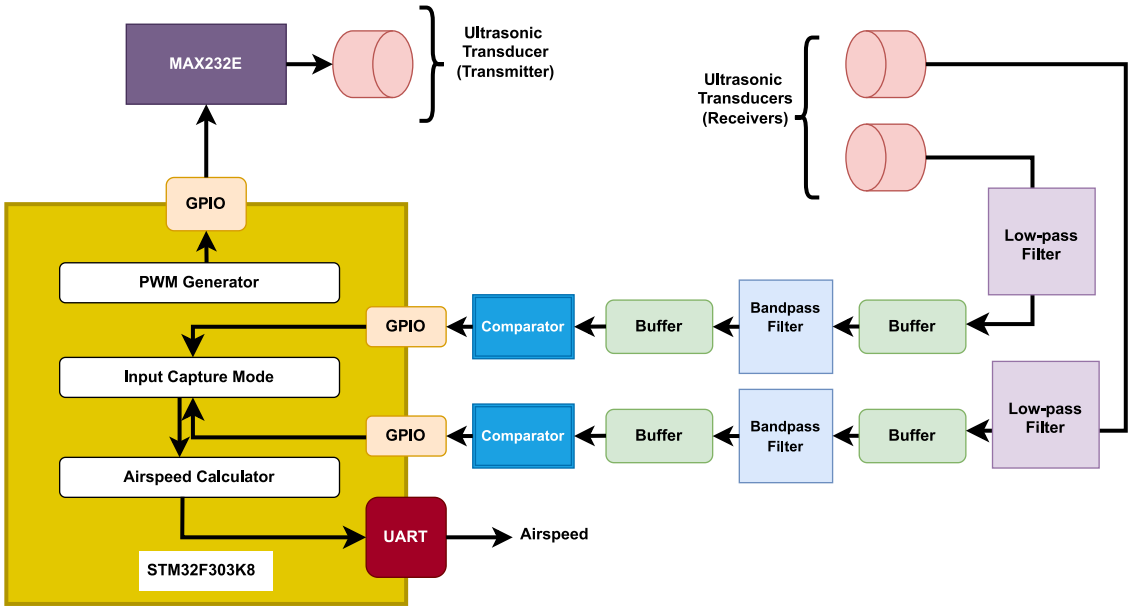

Figure 4.1: *System Block diagram*

The micro-controller uses the general purpose input/output (GPIO) to communicate with all external devices and components, including generating the PWM signal and reading the two amplified square waves from both receivers to be evaluated by the input capture mode.

A detailed view of the circuit components and how they inter-link to each other can be found in Figure A.1.

4.2 Hardware components

The appropriate hardware components are critical in developing an effective and efficient prototype, regardless of the intended applications. The right hardware not only impacts the overall performance and reliability of the project but also influences several crucial factors along the development lifecycle.

4.2.1 Micro-controller

The STM32F303K8 [29] micro-controller, part of the STM32 family, was chosen for the project due to its extensive features and noteworthy advantages contributing to the prototype's overall efficiency, performance, and functionality.

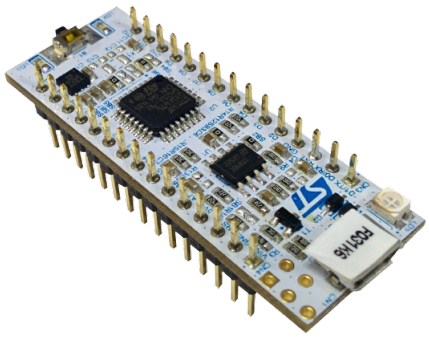

Figure 4.2: *The STM32F303K8 micro-controller*

It is readily available and has all the basic features that satisfy the prototype computational requirements, which include;

- Performance & Computational Capabilities: The micro-controller features a high-performance, 32-bit ARM Cortex-M4 processor with Floating point unit (FPU) running up to 64 MHz. This ensures ample processing power, allowing for quick and accurate computation of the airspeed measurements captured by the ultrasonic sensors without any significant latency.
- Compact Form Factor and Scalability: The micro-controller, with its small footprint, allows for a compact sensor design, making it suitable for applications with limited space or strict size constraints, such as drones. The micro-controller's scalability within the STM32 family offers flexibility in the development process for any potential future enhancements or iterations of the project.

- Power Efficiency: The micro-controller supports multiple low-power modes and a low operating voltage range (between 2.0 and 3.6 V), enabling efficient power consumption and extending the drone's overall battery life when implemented in real-world applications.

4.2.2 Ultrasonic transducers

For the ultrasonic transducers, the EC1404 [30] in Figure 4.3a & Figure 4.3b, transmitter and receiver respectively) were chosen due to their outstanding features and characteristics that make them highly suitable for prototype as compared to the piezo elements in Figure 4.3c. The EC4104 has high sensitivity, high sound pressure levels, good vibration and shock resistance, water resistance and operating well with a resonance frequency of 40 kHz.

(a) **(b)** **(c)**

Figure 4.3: *Ultrasonic transducer types: transmitter and receiver*

On the other hand, the piezo elements (Figure 4.3c) are easier to implement physically in the project due to their thinness and lightweightness. They, however, have a resonance frequency of 6.3 kHz, which puts them well within the normal acoustic hearing range. Therefore, they pick up many frequencies that must be significantly filtered with conventional filtering methods. They are also prone to vibrations, making them respond to false stimuli.

4.2.3 Passive and active component series

For the project's design, careful consideration was given to selecting resistors and capacitors to ensure the desired performance and accuracy. The resistors of the E96 series were chosen, which provided a wide range of available values with tight tolerances. The E96 series allowed for precise matching of resistance values, which is essential for achieving accurate circuit operation. Similarly, the capacitors used were of the E12 series, which provided a sufficient variety of capacitance options. The E12 series capacitors offered a good balance between granularity in available values and reasonable tolerances. By selecting resistors from the E96 series and capacitors from the E12 series, the circuit design was optimized for component availability while maintaining acceptable accuracy and performance.

4.3 Amplification of the transmitter signal

In order to effectively drive the transmitter transducer, a unique approach is required to amplify the PWM signal. Although the MAX232ACPE [31] is traditionally used for RS-232 [32] signal level translations, its capabilities were harnessed to amplify the PWM signal. It is much more convenient than using a dedicated op-amps and transistor networks to amplify the signal, hence lesser components used.

The PWM signal, generated by the microcontroller, with its inherent low voltage and current levels, is insufficient for optimally driving the ultrasonic transducer. By introducing the signal into the MAX232ACPE, we leverage the chip's internal charge pumps to achieve the necessary voltage boost. Simultaneously, the IC's drive capability provides the required current surge, ensuring the transducer is operated at sufficient power.

4.4 Signal reception

The signal reception subsystem is a fundamental component of the ultrasonic sound prototype designed to calculate the airspeed of a fixed-wing drone. This subsystem receives and processes the ultrasonic sound waves reflected from the surroundings. It is critical in acquiring accurate and reliable data necessary for precise airspeed calculation.

One key aspect of the signal reception subsystem is the implementation of various filtering techniques. Filtering is essential to optimize the received signals, eliminate unwanted disturbances, and ensure that only relevant frequency components are processed for airspeed measurement. Filtering techniques help enhance the signal quality, improve the signal-to-noise ratio, and minimize the impact of external noise sources, leading to more accurate and dependable airspeed readings.

4.4.1 Low-pass filter

Using a Low Pass Filter (LPF) as shown in Figure 4.1 in the signal reception subsystem is crucial for removing high-frequency signals that could interfere with the airspeed measurement.

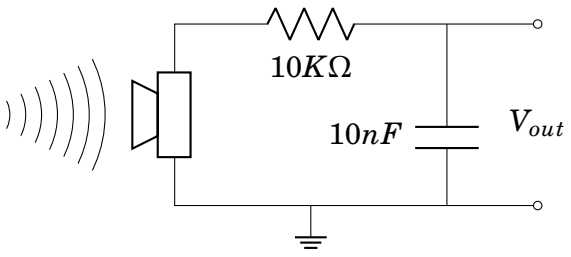

Figure 4.4: *Low-pass filter circuitry*

The LPF minimizes noise where high-frequency noise can impact the accuracy and reliability of the signal. These might emanate from either electromagnetic interference (EMI) or ambient noise, and therefore, facilitate the system to only focus on the desired frequency range. The filter also acts as a signal conditioning mechanism by suppressing the high-frequency disturbances and harmonics that could introduce distortions in the received signal.

The general formula [33] for calculating component values for a passive single-pole filter is;

$$f_c = \frac{1}{2 \times \pi \times R \times C} \tag{4.4.1.1}$$

Where f_c is the cutoff frequency. If we assume a capacitor of 10 nF and f_c to be 40 kHz, then

$$\begin{aligned} 40{,}000\,\text{Hz} &= \frac{1}{2 \times \pi \times R \times 10 \times 10^{-9}} \qquad \text{solving for } R \\ &= 397.89\,\Omega \\ &\approx 470\,\Omega \text{ E96-series} \end{aligned} \tag{4.4.1.2}$$

Given the desired 40 kHz cutoff frequency and a 10 nF capacitor, the ideal resistor value calculates to approximately 470 Ω. However, the practical implementation of electronics often deviates from the ideal due to a myriad of factors including component tolerances. The components introduce parasitic elements like unwanted inductance and capacitance, especially at higher frequencies, which alters the filter's characteristics, potentially making the calculated values less effective.

The choice was to use a 10 kΩ resistor as depicted in Figure 4.4, which provided a steeper roll-off that effectively eliminated the high-frequency signals. Furthermore, a higher resistor value ensures a smaller voltage drop for a given input signal, preserving its amplitude to a greater extent.

4.4.2 Signal buffering

Buffer amplifiers were used in the design to transform electrical impedance from one subsection of the circuit to another. Their main aim was to prevent the signal source from being affected by whatever currents (or voltages) the load may impose.

Typically, current buffer amplifiers transfer current from a first circuit with a low output impedance level to a second circuit with a high input impedance level. An operational amplifier (op-amp) offers several advantages when implementing signal buffering for impedance matching. First and foremost, an op-amp facilitates impedance matching between the source and load, ensuring efficient power transfer without significant signal degradation due to impedance mismatch. Its high input impedance and low output impedance characteristics enable effective isolation of the source from any potential loading effects caused by the load impedance. This impedance-matching capability minimizes signal reflections and maximizes energy

transfer between the source and the load.

In addition to impedance matching, signal integrity preservation is a crucial benefit of using an op-amp as a buffer. The op-amp acts as a buffer between the source and load, effectively isolating the load from the sourcing impedance. This prevents any degradation or distortion of the signal, particularly when dealing with high-frequency signals or varying load impedances. The op-amp buffer ensures accurate and reliable signal processing by maintaining the signal's integrity.

Another advantage of using an op-amp buffer is its amplification capability. The op-amp can provide signal gain, which proves advantageous when the source signal is weak or has a low amplitude. By amplifying the signal before it reaches the load, the op-amp ensures that it receives a sufficiently strong signal for accurate and reliable signal processing.

Op-amps also offer design flexibility in impedance-matching applications. Their gain and output impedance can be adjusted to match specific impedance requirements, allowing for customization of the buffer circuit. This customization optimizes the signal transfer and ensures the buffer meets the impedance-matching needs of the particular system or application. Additionally, op-amps can utilize feedback networks, further refining the buffer's performance and characteristics.

The op-amp buffer provides isolation from load variations, safeguarding the source from any fluctuations in the load impedance. This isolation ensures that changes or variations in the load impedance do not affect the source signal, maintaining signal stability and fidelity throughout the system.

Moreover, op-amp buffers allow for the creation of multiple outputs from a single source signal. This capability accommodates scenarios where various loads of varying impedances must be driven simultaneously. This was particularly useful when probing subsections with an oscilloscope or multi-meter to ensure that no electrical disturbances are introduced while the data is being measured.

4.4.3 Bandpass filter

A bandpass filter allows frequencies within a specific range and rejects or attenuates frequencies outside. It is a cascade of a low pass filter, which ideally isolates the signals that have frequencies higher than the cutoff frequency, and a high pass filter, used to isolate the signals that have frequencies lower than the cutoff frequency.

The procedure for designing the bandpass filter (BPF) is similar to the LPF introduced in subsection 4.4.1. However, there are several things to consider. We saw that in section 2.2, the ultrasonic receiver transducers will be mounted slightly behind the transmitter at a certain angle α. This essentially means that when

a 40 kHz ultrasonic sound wave is emitted from the transmitter, depending on the speed of the platform, the receiver transducers will register a relatively lower frequency of the same sound wave due to the Doppler beam swinging technique. This also means that when designing the BPF, the centre frequency is moved from 40 kHz to an arbitrary frequency of 36 kHz.

The critical factor to consider when dealing with the design of the BPF is the Gain bandwidth (GBW) of the Op-amp in use, which is the product of the amplifier's bandwidth and the gain at which the bandwidth is measured. For devices such as operational amplifiers with a simple one-pole frequency response, the GBW is nearly independent of the gain at which it is measured. Therefore, the roll-off or the steepness of the frequency response of the filter will largely depend on the GBW of the Op-amp. This phenomenon can be seen with the FilterPro Desktop software [34], where a narrower BPF would cause an increase in the GBW. This value is then compared to the Op-amp's datasheet GBW, which can then act as a litmus test to the suitability or usage of the Op-amp to design the filter.

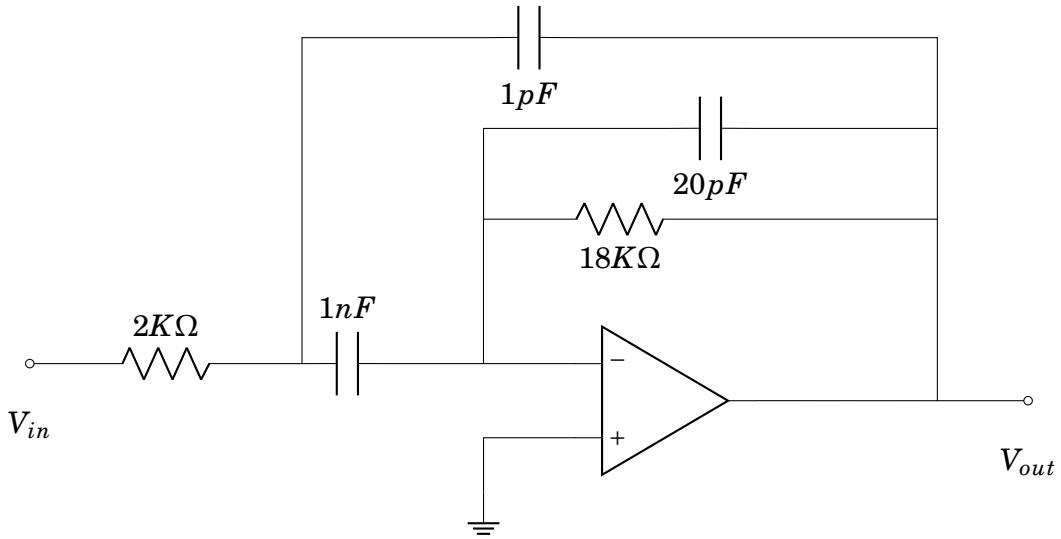

Figure 4.5: *Band-pass filter circuitry*

The active bandpass filter in Figure 4.5 employs an operational amplifier with strategically chosen passive components to achieve the desired frequency response. Though its effect might be subtle in the audio frequency range, such a component can play a pivotal role in shaping the filter's overall response in high-frequency applications. The combination of these high-pass and low-pass sections results in a bandpass behaviour, permitting only a specific band of frequencies to pass while attenuating others outside this range. The specific choice of component values has been adjusted to account for real-world component tolerances, ensuring the filter performs optimally in its intended application.

4.5 Digital Comparator

A comparator IC was explicitly chosen to digitize the signal from the BPF due to its inherent characteristics that make it more suitable for signal digitization than an Op-amp configured in a comparator format. The choice was to use a LM2903P [35], which is a dual voltage comparator that stands out as an advantageous choice over traditional comparators for several key reasons. Its dual-comparator design allows for streamlined circuit implementations, reducing component count. With its wide operating supply voltage range from 2–36 V, it demonstrates versatility across diverse applications.

The LM2903P offers significant advantages over using traditional operational amplifiers as comparators because it is designed specifically for comparison applications, ensuring faster response times and reduced risk of latch-up. Its dual comparator architecture allows for increased efficiency, reducing the need for multiple devices in circuits requiring more than one comparison. Notably, its open collector output provides added flexibility, enabling easier interfacing with various digital systems.

The device's low input offset voltage ensures higher precision when comparing signals, an attribute that might not be as optimized in standard op-amps, which ensures reliability and optimal performance.

4.6 Calculating the airspeed

The STM32F303K8 micro-controller incorporates an input capture feature that enables frequency measurement of an external waveform. This functionality relies on timers and capture-compare channels within the micro-controller.

The timer is configured appropriately with the desired prescaler, period, and other parameters to use input capture. A specific capture compare channel is then assigned for input capture, responsible for capturing timestamps of the waveform's rising and falling edges. The micro-controller's input capture unit is set to detect the desired edge(s) which when triggered, captures the current value of the timer's counter register associated with the configured capture compare channel. By capturing the timestamps of two consecutive edges, the micro-controller calculates the period by measuring the elapsed time between them. The frequency is then calculated as the inverse of the period.

To calculate the airspeed using the estimated frequency from the Doppler swinging technique Equation 2.2.9, one can obtain the frequency shift Δf, from which the airspeed can be calculated.

4.7 Cost estimation

This section provides an in-depth analysis of the anticipated expenses and financial considerations associated with the project. To effectively plan and execute the project, it is crucial to have a comprehensive understanding of the resources and funds required

	Qty.	Item	Cost (kr)	Vendor
1.	1.	STM32F303K8	126	Farnell
2.	1.	T_x transducer	59	Elektrokit
3.	2.	R_x transducer	118	Elektrokit
4.	3.	MCP6002 Op-amp	36	Elektrokit
5.	1.	LM2903P Dual Comparator	9kr	Elektrokit
7.	1.	Ceramic Capacitors	145	Amazon
8.	1.	Resistors	159	Elektrokit
10.	2.	Breakboards	119	Amazon
11.	5.	Connecting wires	60	Elektrokit
12.	1.	Potentiometers	193	Amazon
13.	1.	MAX232ACPE	120	Electrokit
		Total	1568	

Table 4.1: *Cost estimation per item*

To reach the objective of designing a low-cost prototype, a carefully curated list of cost-effective components shown in Table 4.1, that both were on a budget and successfully met the technical requirements of the prototype, were considered.

The heart of our design was centered around the STM32F303k8 micro-controller unit, a relatively affordable yet powerful micro-controller. Its price point was reasonable, ensuring the system's core was financially and technologically feasible. Additionally, additional electronics components consisted of three MCP6002 [36] dual operational amplifiers, one LM2903P comparator, a set of indispensable capacitors and resistors, and various potentiometers to adjust levels within the system. All these components were chosen for their excellent value in cost and functionality.

The ultrasonic system comprises one ultrasonic transmitter (T_x) and two ultrasonic receivers (R_x) transducers. These devices were the "eyes and ears" of the system, necessary to calculate airspeed. Given the design constraints, they were specifically chosen for cost and their well-suited performance characteristics.

A non-negligible part of the cost consideration was the assembly materials. Here, two breadboards and an array of wires for component placement and signal routing

were assembled. These were selected considering their economical price and accessibility. Moreover, the platform holding the components was 3D printed to keep down the prototype's cost. This not only allowed for the production of a custom design that optimally arranged the components in a reasonable manner but also meant the cost of the structural base was very affordable as only the price of the printing material was considered.

By judiciously choosing both the components and assembly materials, a cost-effective prototype solution was designed that served the purpose of our project without compromising on performance.

4.8 Sensor positioning

At the heart of our sensing mechanism is the transducer arrangement, which plays a pivotal role in capturing real-time data. Figure A.1 provides a top-down view of the platform where the transmitting transducer and two receiving transducers are strategically placed. This arrangement is optimized for maximum data capture accuracy while ensuring minimal interference.

A few general considerations exist when determining the best placement for the transducers. Firstly, avoiding obstructing the drone's normal operation or affecting its aerodynamics is important. The transducers should be positioned to allow unobstructed airflow and not interfere with the drone's stability and maneuverability.

Secondly, optimal coverage and range should be considered. The placement should be chosen to provide the desired coverage area and range for the ultrasonic sensors. The field of view required for the application should be considered, ensuring the transducers have a clear line of sight to the targets they need to detect or monitor.

Vibration and noise isolation also play a significant role. Mounting the transducers in a location that minimizes vibrations and noise helps improve the accuracy and reliability of the readings. Vibrations and noise can potentially interfere with the sound waves emitted by the transducers and impact their ability to accurately detect and measure distances.

Considering these factors, a common placement for ultrasonic transducers on a fixed-wing drone is typically underneath the drone's body or fuselage. This location provides a relatively unobstructed field of view and allows for easy integration with the drone's power and data systems.

For practical and iterative testing methodology, a bicycle was utilized as a test platform, given its accessibility and easy of modification compared to testing on a real fixed-wing drone. As depicted in Figure A.3, the transducer platform is securely

affixed to a bicycle, ensuring stability even during movement. Alongside the platform, a digital anemometer is mounted to gather data on airspeed, enhancing the interpretation of the data from the transducers. The bicycle-based setup allowed for a more flexible and hands-on approach to interactively rest and make adjustments.

5

Results

In this section, a presentation of the results obtained during the study and the design of the prototype is given. A series of experiments and analyses were conducted to evaluate the effectiveness and feasibility of the prototype.

5.1 Micro-controller configuration

During the study, the micro-controller (Figure 4.2) was configured to run the system clock at 64 MHz. To generate the required PWM signal, the PWM mode with a specific prescalar value and period was configured on the periphery of TIM1, channel 1. This configuration allowed for the control of the ultrasonic transducer succinctly. The prescalar value was set to 0, and the period of the TIM1 periphery was set at 1582. This resulted in a precise 40 kHz PWM square wave at the GPIO pin PA0.

5.2 Processing the received signal

Ultrasonic transducer receivers typically receive a sinusoidal waveform because they are designed to detect and measure ultrasonic frequencies. A sinusoidal waveform, also known as a sine wave, is a fundamental waveform often used to represent periodic oscillations.

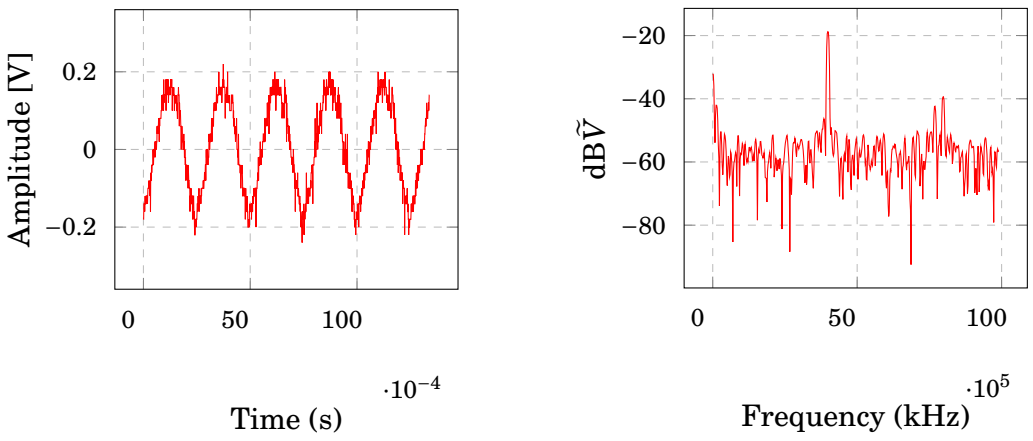

(a) *Time-domain*

(b) *Spectral analysis*

Figure 5.1: *Raw unfiltered signal from the receiver*

The signal shown in Figure 5.1a shows real data captured from one of the ultrasonic transducer receivers. Although the transducer has a frequency response as shown in Figure 2.7, the transducer resonates and picks up frequencies closer to the fundamental frequency, leading to noise aggregates and decreasing the signal-to-noise ratio (SNR). Looking at Figure 5.1b, a spectral analysis view of the frequency domain shows that the SNR is quite high, but because the signal will be filtered and further processed, it needs to be amplified beyond the 400 mV as seen in Figure 5.1a, so that it can be improved or cleaned-up before being digitized.

5.2.1 Low-pass design

Several considerations were taken into account during the Low Pass Filter (LPF) design process. One of the critical factors was the choice of the cut-off frequency. In this case, a cut-off frequency slightly above 40kHz to 42kHz was selected. This decision was primarily driven by the tolerances of the components used in the filter.

By setting the cut-off frequency in this range, the LPF effectively attenuates frequencies above 41 kHz while allowing lower frequency signals to pass through, as seen in Figure 5.2. This design choice ensures that high-frequency noise or unwanted signals are adequately filtered out while still maintaining the desired signals within the passband.

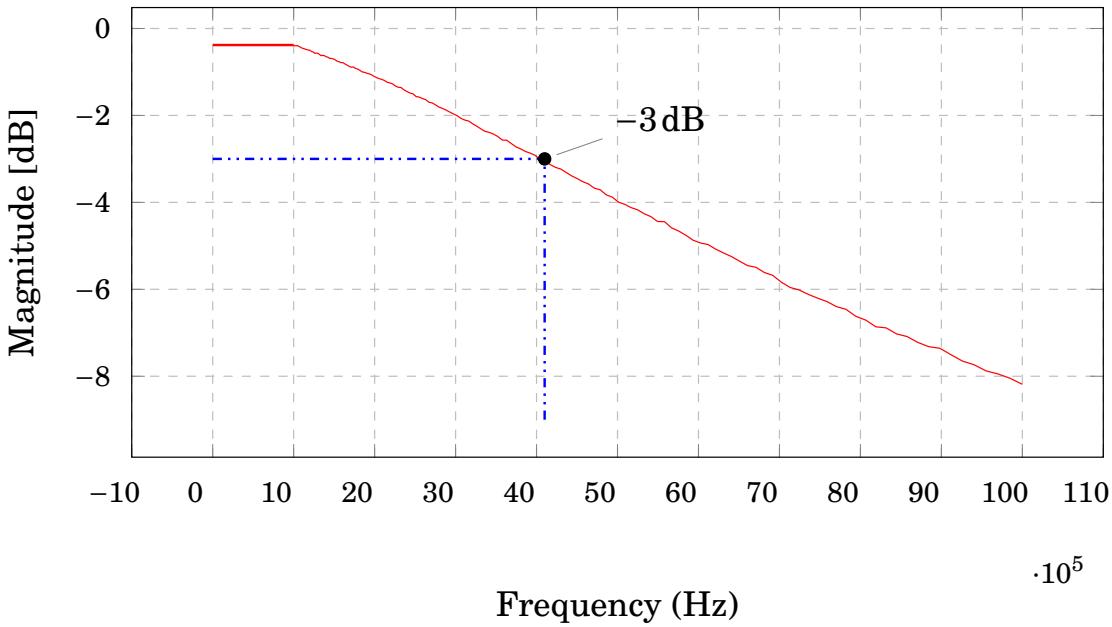

Figure 5.2: *Frequency response bode plot from the low-pass filter*

5.2.2 Bandpass filtering and amplification

The received signal should be amplified to significant levels before digitising it in some form or shape. This requires active and passive components, preferably op-amps together, to get a cleaner signal and reduce the noise levels it contains.

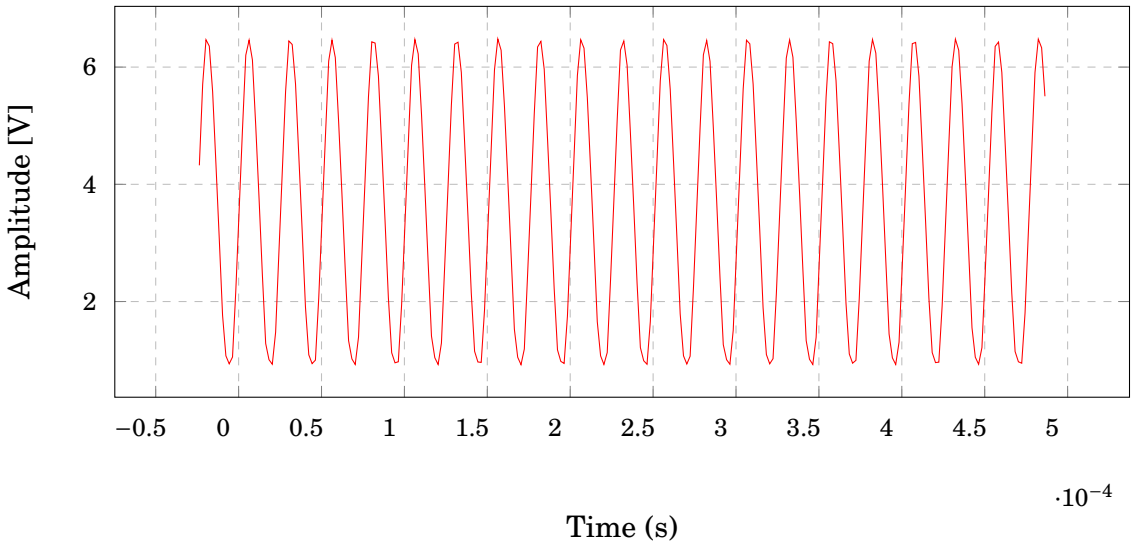

(a) *Time-domain*

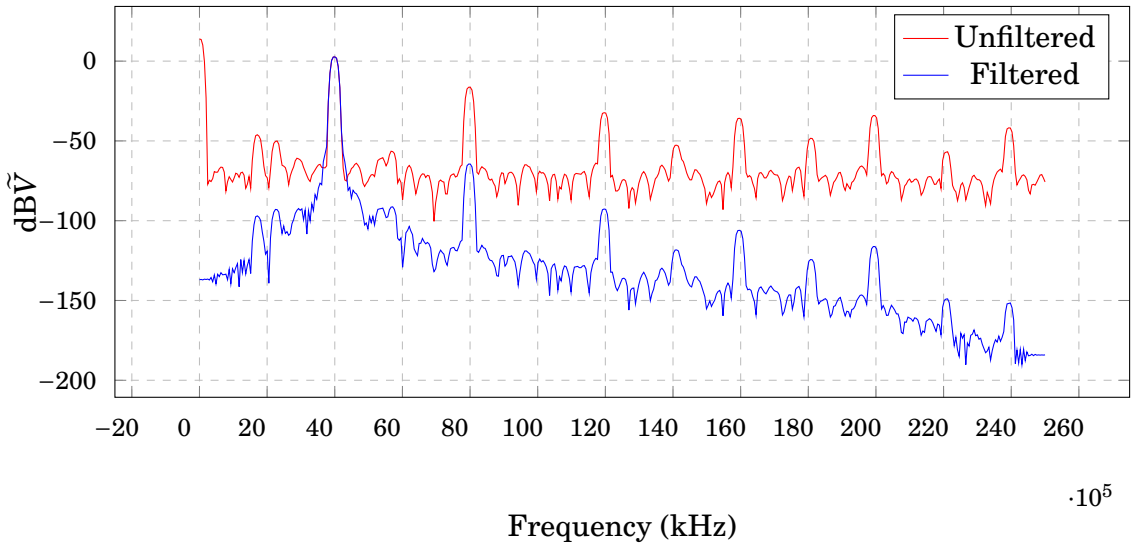

(b) *Bandpass filter frequency response while the system is at rest*

Figure 5.3: *Filtered and unfiltered signal representation*

Comparisons between the two signals in Figure 5.1a and Figure 5.3a show an increase in the peak-to-peak voltage, amplifying the signal enough to work with. At first glance, it looks as if the signal is clean enough to be digitized. But when it is viewed in the frequency domain, the unfiltered signal in Figure 5.3b shows that apart from the fundamental frequency of about 40 kHz that we are interested in, there is a presence of other frequencies aggregated together with it, although with lesser magnitude.

By passing the signal through a bandpass filter with lower and upper cutoff frequencies of between 38–40 kHz respectively, the magnitude of unwanted frequencies is significantly decreased, as seen in the filtered signal of Figure 5.3b. Subsequently, the noise levels decrease, thus improving SNR.

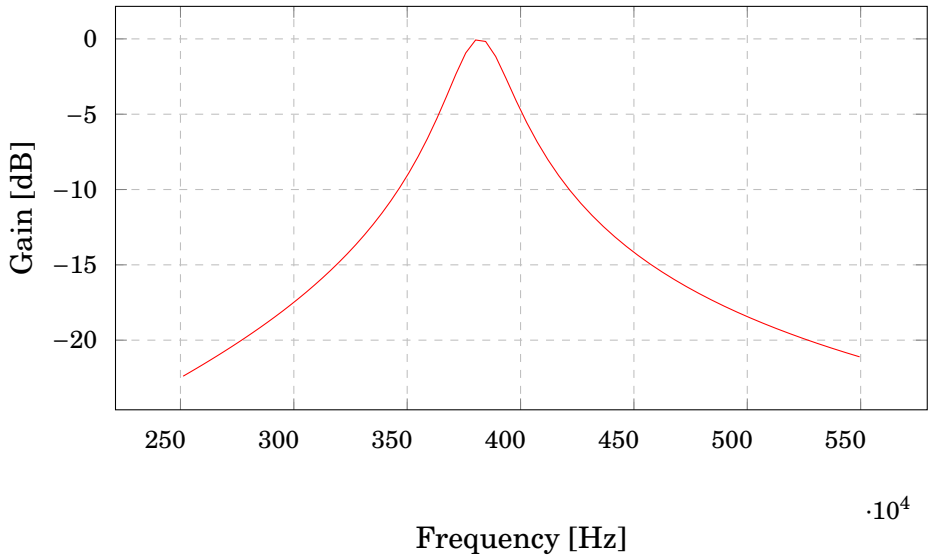

Figure 5.4: *Frequency response curve of the designed bandpass filter*

Figure 5.4 illustrates the frequency response or bode plot of the bandpass filter, showing a gain of approximately 1 dB. This indicates minimal amplification or attenuation of the input signal within the passband region, ensuring that the desired 38 kHz centre frequency signal remains largely unaffected while unwanted frequencies are diminished.

The filter's center frequency is set at 38 kHz, making it sensitive to signals around this frequency and allowing them to pass through efficiently. This specific setting helps in isolating and focusing solely on the desirable signals by filtering out nearby unwanted frequencies. The design also incorporates an allowable passband ripple of 1 dB, further ensuring consistent gain levels for frequencies within the passband, contributing to accurate signal processing.

The passband width is set to 2.5 kHz, allowing frequencies around the center frequency to pass with minimal attenuation. This narrow passband width emphasizes a specific range of frequencies, efficiently attenuating signals outside this scope.

For the stopband specifications, the filter features a 1 kHz stopband width, ensuring significant attenuation of frequencies beyond the passband limits and suppressing potential interference or noise signals near the passband edges. A stopband attenuation set at −45 dB effectively minimizes the impact of frequencies falling outside the passband range on the output.

Following the Butterworth filter response, the bandpass filter, designed with an order of 2, guarantees a maximally flat passband with minimized ripple. This choice allows for a smooth transition between the passband and stopband regions, safeguarding the desired signal integrity.

In terms of topology, the bandpass filter employs the Multiple Feedback configuration. This option was preferred for its efficiency in achieving the desired filter response with fewer components, ensuring a simple yet effective filter design for optimal signal processing.

5.2.3 Digitizing the signal

When digitizing a signal, the process involves converting continuous analog signals into discrete digital representations. One method to achieve this transformation is by using a dedicated integrated circuit, such as a comparator, to convert a sine wave into a square wave.

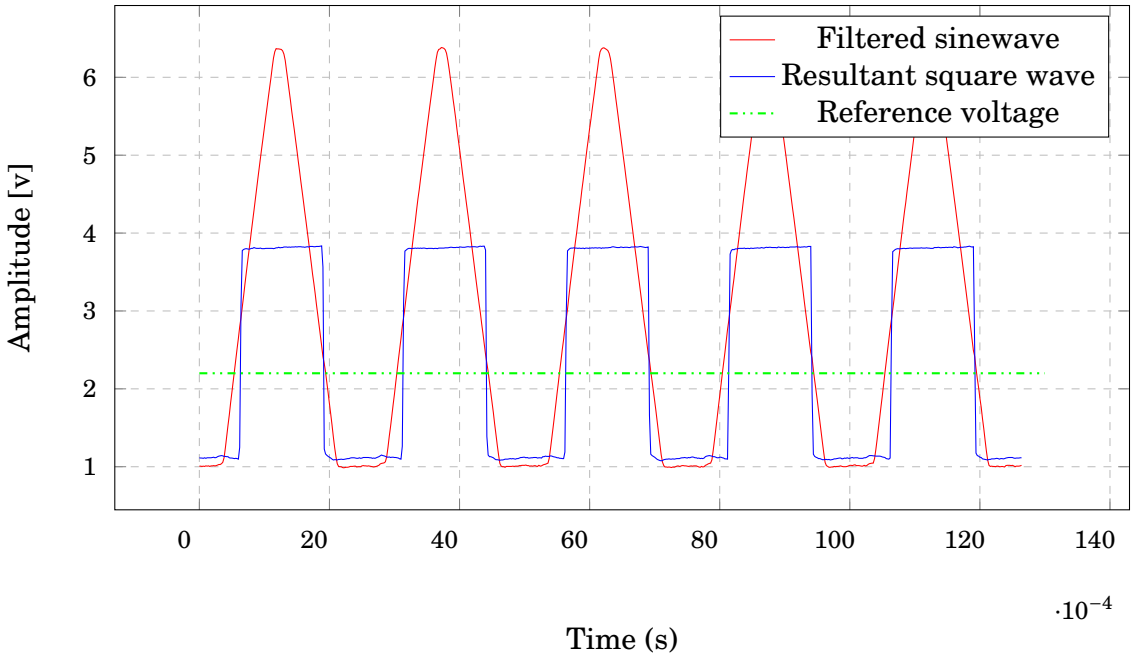

Figure 5.5: *Converting sine wave to square wave*

A filtered sine wave, as referenced in Figure 5.6, is processed using this integrated circuit (IC). Functioning as a comparator, it evaluates the instantaneous voltage level of the input sine wave against a fixed reference voltage of 2.3 V. This comparison results in the output of a binary square wave that alternates between high and low logic values, yielding a low-resolution approximation of the original sine wave.

With this approach, the continuous amplitude variations of the sine wave are compartmentalized into four discrete levels or bit combinations: 00, 01, 10, 11. However, this approach is not without its limitations. There's a discernible loss of amplitude information, with the finer variations of the sine wave approximated to the closest of the four discrete values, and thereby introducing quantization errors and potential distortion.

5.3 Calculated the airspeed

The speed of a fixed-wing drone can be calculated using ultrasonic sound through the Doppler beam swinging technique. For the experimental setup, the transmitter transducer was strategically placed at the front of the drone model, and two receiver transducers were located slightly behind it, positioned at an angle of 60° relative to each other. This positioning facilitated the capturing of reflected sound waves. Periodically, at intervals of two seconds, and the transmitter transducer emitted pulsed ultrasonic sound waves at a base frequency of 40 kHz.

The essence of this technique lies in analyzing the Doppler shift caused by the platform. As the drone moved, the relative frequency change induced by it against its direction of movement became more pronounced. When wind speeds were assessed, which ranged between 1–30 $\mathrm{m\,s^{-1}}$, it was observed that due to the Doppler effect, the reflected waves' frequency showed a decline compared to the transmitted frequency. Given the inputs from the two receiver transducers, the measured frequencies from both were averaged to provide a more reliable airspeed reading.

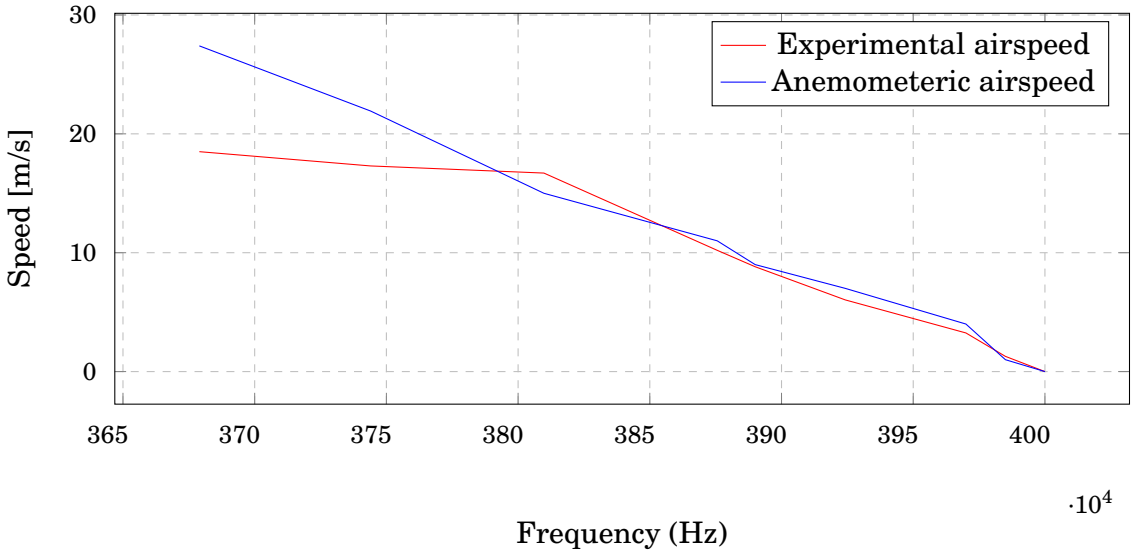

Figure 5.6: *Calculated airspeed vs. anemometer speed reading*

A review of the data in Figure 5.6 indicates a correlation between declining frequency values and increasing airspeeds. This supports the assertion that ultrasonic sound can accurately gauge the airspeed of a fixed-wing drone. However, it's crucial to understand the limitations. The sensitivity of the transducers plays a pivotal role. Specifically, transducers exhibit maximum sensitivity at their designated frequency response. Any deviation, especially frequencies lower than this threshold as seen in the figure above, causes the transducer to behave akin to a bandpass filter. This effect attenuates some frequencies, potentially impacting the precision of the desired airspeed calculation.

6

Conclusion

This thesis has explored the feasibility of measuring airspeed using an ultrasonic technique. While this method offers certain advantages, such as non-intrusiveness and the ability to measure airspeed remotely, it has limitations that must be considered.

One limitation is the upper-speed limit at which the ultrasonic technique can accurately measure airspeed. Due to the nature of ultrasonic transducers, their frequency response puts that limitation. As the object being measured moves at higher speeds, the Doppler effect can cause frequency shifts that may exceed the range detected by the ultrasonic transducer. This limitation restricts the maximum speed at which the airspeed can be reliably measured using ultrasonic techniques.

Furthermore, when considering practical implementation, wider-band ultrasonic transducers are an option. However, these transducers can be more expensive to acquire and heavier, making them less suitable for airborne applications such as drones. The added weight and complexity can hinder the drone's performance and flight capabilities.

Given these limitations, it is important to assess alternative methods for airspeed measurement. Several alternative approaches exist, such as hot-wire anemometry or optical methods. These techniques offer different advantages and limitations and may be more suitable for specific applications or speed ranges. It is recommended to explore these methods and carefully consider their suitability based on the specific requirements of the airspeed measurement task.

In conclusion, while the ultrasonic technique has demonstrated potential for a low-cost, true airspeed measurement prototype, its limitations concerning speed range, frequency response, and practical implementation must be considered. It is essential to carefully evaluate the requirements and constraints of the application and consider alternative methods to determine the most appropriate approach for accurately and reliably measuring airspeed.

7

Future work

The most important improvement that can be made is to consider alternative methods for implementing filters in the system. Analog filters can pose challenges due to component tolerances and availability, making their implementation difficult and unreliable. However, advancements in technology have provided alternatives that may overcome these limitations.

One potential solution is to leverage a high-quality Analog-to-digital converter (ADC) capable of sampling at least the resonance frequency of the ultrasonic transducer in use. For instance, the maximum frequency expected from the ultrasonic transducers used in this project should not be greater than 40 kHz. This implies that any ADC chosen should have at least twice the sampling frequency to fulfil the Nyquist criterion. By utilizing a high-performance ADC, it becomes feasible to implement digital filters such as FIR or IIR filters. These digital filters can achieve significantly higher orders than their analog counterparts, allowing for more precise and accurate signal processing.

The advantage of employing digital filters is overcoming component limitations and achieving greater control over the filter characteristics. Unlike analog filters, digital filters do not rely on physical components with tolerances, which can introduce errors and affect performance. Instead, digital filters operate through algorithms, allowing precise tuning and control. Furthermore, digital filters offer the advantage of lower power consumption compared to analog filters.

Regarding transmitting ultrasonic sounds, it is worth considering the usage of the AD9833 [37] waveform generator for generating sinusoidal sound waves in the airspeed measurement system. The AD9833 programmable waveform generator IC offers precise control over frequency and phase but without amplitude. By utilizing the AD9833, it becomes possible to generate high-quality sinusoidal waves better suited for airspeed measurement than square waves. Square waves contain multiple harmonics that can introduce unwanted frequency components and distortions, which may affect the accuracy of the measurements. In contrast, sinusoidal waves have a more straightforward and cleaner harmonic content, allowing for more accurate and reliable airspeed measurements.

A pull-up network can be employed to increase the signal amplitude and power.

This network consists of PNP and NPN transistors that configure the output stage of the AD9833, effectively increasing the current and voltage levels of the generated sinusoidal wave. By boosting the signal strength, the pull-up network ensures that the ultrasonic transducer receives a sufficient power level for optimal performance.

The effect of temperature on the speed of sound was introduced in section 2.5. However, this prototype assumes a constant room temperature of 25°C. Therefore, it is imperative to include real-time temperature calculations from the beginning to try to mimic the real-world conditions in which the prototype will operate.

In the event of stemming interference from other ultrasonic transmitters, incorporating digital modulating techniques like amplitude shift keying (ASK) can be applied. This technique provides robustness against interference because it utilizes distinct signal characteristics that are less likely to be affected by interference sources operating at different frequencies or with different amplitudes or phases. Additionally, techniques like error correction coding and interleaving can be employed to improve the system's ability to recover the original data in the presence of interference. These methods introduce redundancy and ensure that even if some bits are corrupted by interference, the original information can still be accurately reconstructed.

Bibliography

[1] Kai Lehmkuehler. "A Direct Comparison of Small Aircraft Dynamics between Wind Tunnel and Flight Tests". In: (2016-09-28). DOI: http://hdl.handle.net/2123/16511.

[2] Tom Bensson. *What is weight?* URL: https://www1.grc.nasa.gov/beginners-guide-to-aeronautics/weight-gravitational-force/.

[3] Federal Aviation Administration. "Chapter 8: Flight Instruments". In: *Pilots Handbook of Aeronautical Knowledge: Faa-H-8083-25C*. Aviation Supplies amp; Academics, 2023. URL: https://www.faa.gov/regulations_policies/handbooks_manuals/aviation/faa-h-8083-25c.pdf.

[4] Edward L. Houghton and P. W. Carpenter. In: *Aerodynamics for Engineering Students*. Butterworth Heinemann, 2001, p. 233. ISBN: 0750651113. URL: https://soaneemrana.org/onewebmedia/Aerodynamics--Houghton&Carpenter.pdf.

[5] Momchil Makaveev, Mirjam Snellen, and Ewoud J J Smeur. *Microphones as airspeed sensors for unmanned aerial vehicles*. Feb. 2023. URL: https://www.ncbi.nlm.nih.gov/pmc/articles/PMC10007234/.

[6] Hiroyuki Nakamura et al. "Measurement of Actual Vehicle Speed Using Ultrasonic Doppler Effect". In: *Japanese Journal of Applied Physics* 29.S1 (Jan. 1990), p. 228. DOI: 10.7567/JJAPS.29S1.228. URL: https://dx.doi.org/10.7567/JJAPS.29S1.228.

[7] G. Voulgaris and J. H. Trowbridge. "Evaluation of the Acoustic Doppler Velocimeter (ADV) for Turbulence Measurements*". In: *Journal of Atmospheric and Oceanic Technology* 15.1 (Feb. 1998), p. 272. DOI: 10.1175/1520-0426(1998)015<0272:EOTADV>2.0.CO;2.

[8] Randal W. Beard and Timothy W. McLain. *Small unmanned aircraft theory and practice*. Princeton University Press, 2012. ISBN: 978-0691149219.

[9] Giancarlo Lopes et al. "Development of 3-D Ultrasonic Anemometer With Nonorthogonal Geometry for the Determination of High-Intensity Winds". In: *IEEE Transactions on Instrumentation and Measurement* PP (July 2017), pp. 1–9. DOI: 10.1109/TIM.2017.2714438.

[10] Michael P. Norton and Dennis G. Karczub. *Fundamentals of noise and Vibration Analysis for Engineers*. Cambridge Univ. Press, 2007. ISBN: 9781139163927. DOI: doi:10.1017/CBO9781139163927.

[11] Pijush K. Kundu, Ira M. Cohen, and David R. Dowling. *Fluid mechanics*. Academic Press, 2016. ISBN: 978-0-12-405935-1. DOI: https://doi.org/10.1016/C2012-0-00611-4.

[12] T. Raju Damarla, P. Karpur, and P.K. Bhagat. “A self-learning neural net for ultrasonic signal analysis”. In: *Ultrasonics* 30.5 (1992), pp. 317–324. DOI: https://doi.org/10.1016/0041-624X(92)90006-8.

[13] Andrew B. Raine et al. “Development of an Ultrasonic Airflow Measurement Device for Ducted Air”. In: *Sensors* 15.5 (2015), pp. 10705–10722. ISSN: 1424-8220. DOI: 10.3390/s150510705. URL: https://www.mdpi.com/1424-8220/15/5/10705.

[14] Ali Ghahramani et al. “Measuring Air Speed With a Low-Power MEMS Ultrasonic Anemometer via Adaptive Phase Tracking”. In: *IEEE Sensors Journal* PP (June 2019), pp. 1–1. DOI: 10.1109/JSEN.2019.2920648.

[15] N. Giordano. *College Physics: Reasoning and Relationships*. Cengage Learning, 2009. ISBN: 978-0840058195. URL: https://books.google.se/books?id=BwistUlpZ7cC.

[16] MARKUS POESSEL. *Waves, motion and frequency: The Doppler effect*. 2011. URL: https://www.einstein-online.info/en/spotlight/doppler/.

[17] Henderson Tom. *Physics tutorial: The Doppler effect*. 2017. URL: https://www.physicsclassroom.com/class/waves/Lesson-3/The-Doppler-Effect.

[18] Tim Freegarde. In: *Introduction to the Physics of Waves*. Cambridge University Press, 2012, pp. 286–290. ISBN: 978-9078677109. DOI: 10.1017/CBO9781139048149.022.

[19] Elham Pirnia. Sept. 2013. URL: https://lup.lub.lu.se/luur/download?func=downloadFile&recordOId=4175205&fileOId=4175207.

[20] Tatiana Kelemenová, Ondrej Benedik, and Ivana Koláriková. “SIGNAL NOISE REDUCTION AND FILTERING”. In: *Acta Mechatronica* 5 (June 2020), pp. 29–34. DOI: 10.22306/am.v5i2.65.

[21] DEWESoft d.o.o. *Signal filtering, signal suppression, signal processing: Dewesoft*. URL: https://training.dewesoft.com/online/course/filters.

[22] Dale Ensminger and Leonard J. Bond. “Design of hltrasonic horns for high power applications”. In: *Ultrasonics: Fundamentals, technologies, and applications*. CRC Press, 2012, pp. 192–193. ISBN: 978-0824758899.

[23] S.C. Abrahams and K. Nassau. “Piezoelectric Materials”. In: *Concise Encyclopedia of Advanced Ceramic Materials*. Ed. by RJ BROOK. Oxford: Pergamon, 1991, pp. 351–354. ISBN: 978-0-08-034720-2. DOI: https://doi.org/10.1016/B978-0-08-034720-2.50097-6.

[24] Samuel Ling, Jeff Sanny, and William Moebs. “Sound”. In: *University physics*. OpenStax, 2021, pp. 823–868. ISBN: 978-1-947172-20-3.

[25] *LTspice Information Center | Analog Devices*. URL: https://www.analog.com/en/design-center/design-tools-and-calculators/ltspice-simulator.html.

[26] *HCS-R04 - SparkFun Electronics*. URL: https://www.sparkfun.com/products/15569.

[27] Oct. 2013. URL: https://www.st.com/en/development-tools/stm-studio-stm32.html.

[28] Sam K. *Analog Discovery 2 Reference Manual*. URL: https://digilent.com/reference/test-and-measurement/analog-discovery-2/start.

[29] STMicroelectronics. *STM32F303K8 Datasheet*. Accessed: 2023-10-09. 2023. URL: https://www.st.com/resource/en/reference_manual/rm0316-stm32f303xbcde-stm32f303x68-stm32f328x8-stm32f358xc-stm32f398xe-advanced-armbased-mcus-stmicroelectronics.pdf.

[30] *EC4014 reference manual*. URL: https://www.electrokit.com/uploads/productfile/41000/07302862.pdf.

[31] *MAX232ACPE reference manual*. URL: https://www.digikey.com/en/products/detail/analog-devices-inc-maxim-integrated/MAX232ACPE/947829.

[32] *The fundamentals of RS-232 serial communication*. Nov. 2022. URL: https://www.analog.com/en/technical-articles/fundamentals-of-rs232-serial-communications.html.

[33] John Clayton Rawlins. "CHAPTER 6 - Capacitance". In: *Basic AC Circuits (Second Edition)*. Ed. by John Clayton Rawlins. Second Edition. Burlington: Newnes, 2000, pp. 171–215. ISBN: 978-0-7506-7173-6. DOI: https://doi.org/10.1016/B978-075067173-6/50007-9.

[34] *FilterPro Desktop Software*. URL: https://www.ti.com/cn/lit/pdf/sbfa001.

[35] *LM2903P reference manual*. URL: https://www.electrokit.com/produkt/lm2903p-dip-8-dual-komparator.

[36] *MCP6002 reference manual*. URL: https://www.microchip.com/en-us/product/MCP6002.

[37] *AD9833 reference manual*. URL: https://www.analog.com/media/en/technical-documentation/data-sheets/AD9833.pdf.

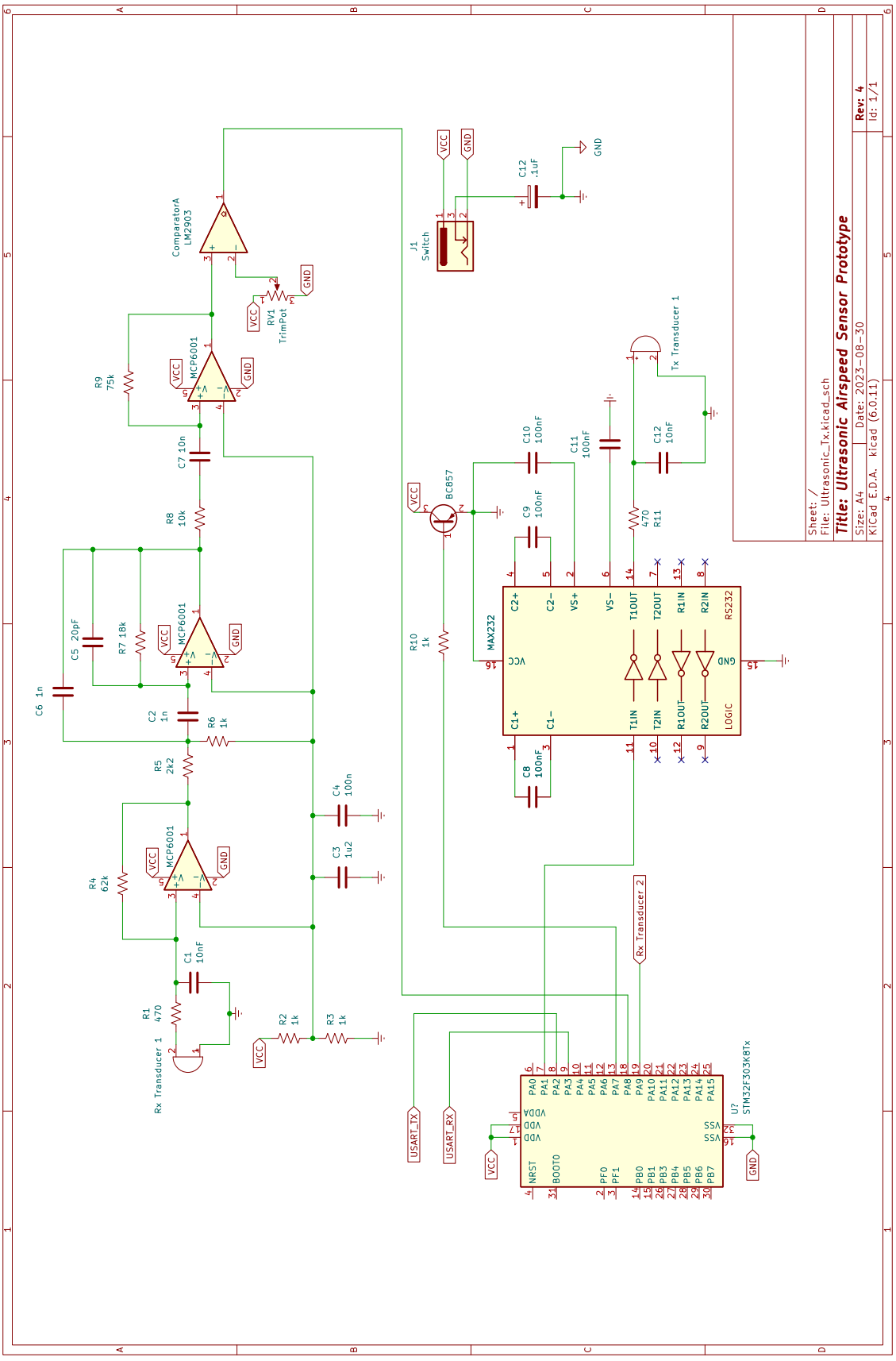

Figure A.1: *Schematic for the sensor prototype*

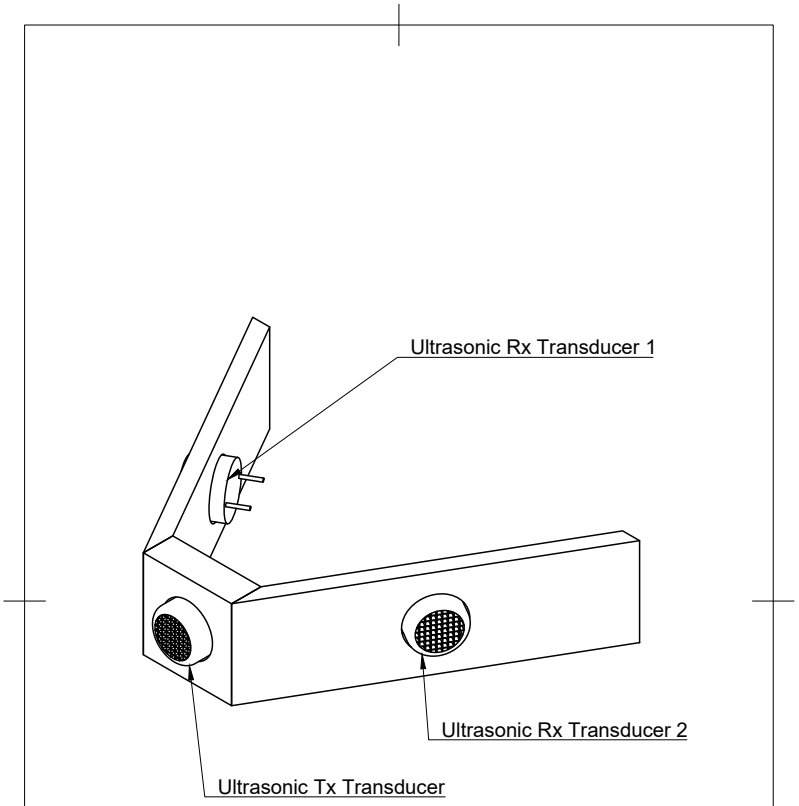

Figure A.2: *Ultrasonic transducers' housing*

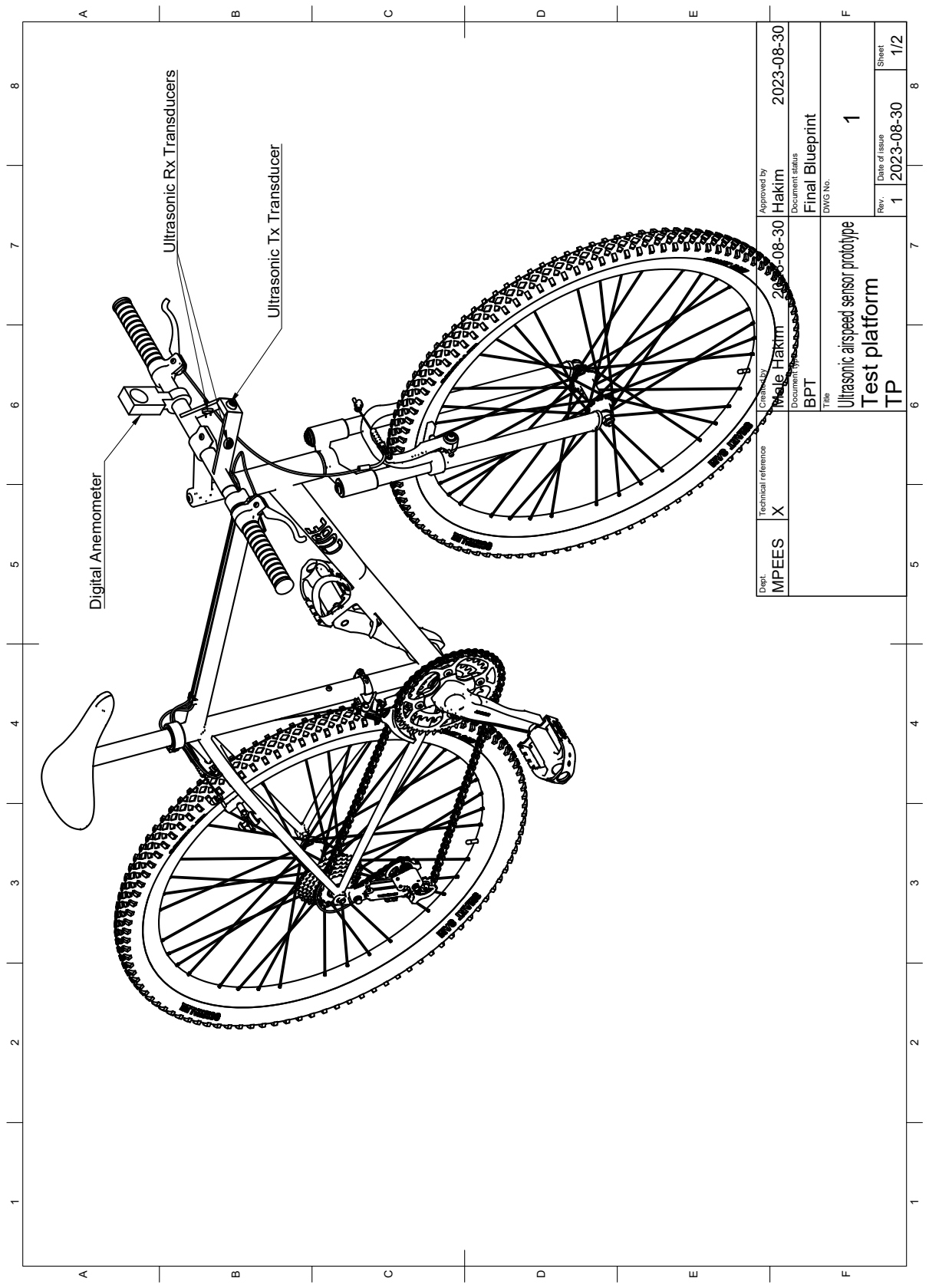

Figure A.3: *Test platform onto which the housing was mounted*